Sudan University for Science & Technology

College of Graduate Studies

Application of Fat Suppression Effect in MRI

تطبيق تثبيط تأثير الدهون في صور الرنين المغنطيسي

A thesis Submitted for the Fulfillment of partial Requirement of M.Sc. in Biomedical Engineering

Prepared By:

Marwa Ahmed Abdelwhab Mohammed

Supervisor:

Dr. Mohammed AL Bashir

2017

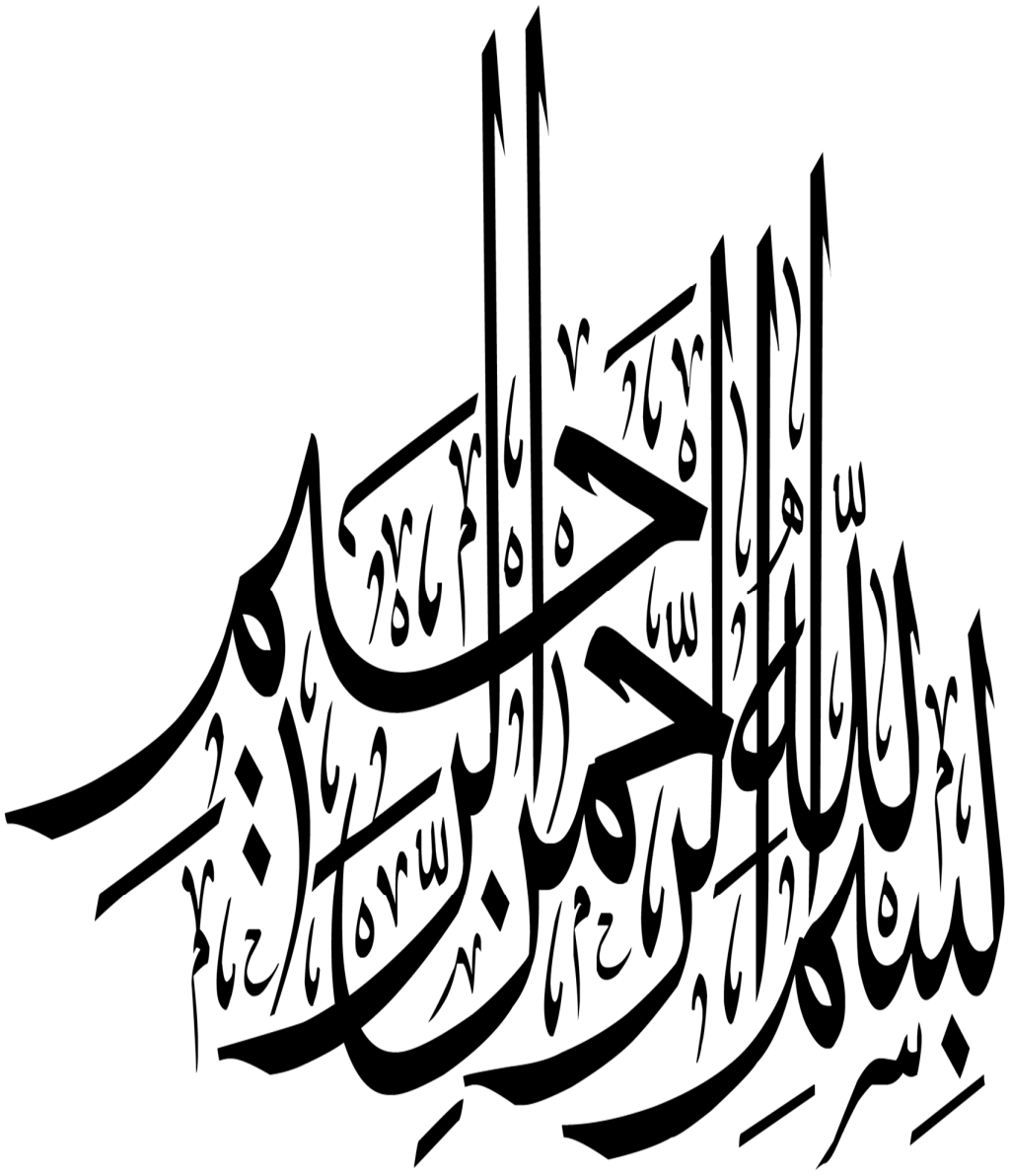
بسم الله الرحمن الرحيم

الاستهلال

قال تعالى:

بسم الله الرحمن الرحيم

قَالَ رَبِّ اشْرَحْ لِي صَدْرِي (25) وَيَسِّرْ لِي أَمْرِي (26)
وَاحْلُلْ عُقْدَةً مِنْ لِسَانِي (27) يَفْقَهُوا قَوْلِي (28))

صدق الله العظيم

سورة طه (25) – (28)

Dedication

I dedication my Research work to my family and many friend and class mate

I dedicate to my mother, father and my husband who they have never left my side.

Acknowledgment

Thanks to Allah the almighty in all time who help me to accomplish this research.

I would also like to show my gratitude to Sudan University of Science and Technology that has given me chance to study the I would than my supervisor Dr. Mohammed AL Bashir

Abstract

Magnetic resonance imaging is one of the most important diagnostic tools of modern healthcare. The signal in medical MRI predominantly originates from water and fat molecules. Separation of the two components into water-only and fat-only images can improve diagnosis, and is the premier non-invasive method for measuring the amount and distribution of fatty tissue.

Fat-water imaging (FWI) enables fast fat/water separation by model-based estimation from chemical shift encoded data, such as multi-echo acquisitions. Qualitative FWI is sufficient for visual separation of the components, while quantitative FWI also offers reliable estimates of the fat percentage in each pixel. The major problems of current FWI methods are long acquisition times, long reconstruction times, and reconstruction errors that degrade image quality(Berglund 2011).

The relationship between phantom structure and composition of density can observe on the three deferent composition of (oil, water. Oil &water), the MRI has many advanced techniques needed to be applied and used in Sudan to advance diagnosis and therapy, the methodology adopted were experiment the three phantoms under spin technique and advance technique and monitor the analyzed image, we found that the advanced technique has more accurate results than the spin, the conclusion of this research that the diagnosis can be more precise by using the MRI advance technique.

مستخلص البحث

يعتبر التصوير بالرنين المغناطيسي احدى اهم مقومات التشخيص الطبي في الرعاية الصحية الحديثة .إشارة التصوير بالرنين المغناطيسي الطبي تنتتج من جزيئات الماء والدهون.

فصل المكونين في الصور المياه فقط والدهون فقط يمكن أن يحسن التشخيص، وهو الأسلوب غير المضر لقياس كمية وتوزيع الأنسجة الدهنية.

التصوير المياه _الدهون تمكن الدهون _المياه من فصل سريع من خلال نموذج قائم على التوقع من خلال عملية الازاحة الكيميائية المشفرة مثل عمليات الالتقاط متعددة الصدى .تصوير الماء _دهون النوعي يكافئ الفصل البصري للمكونات، في حين تصوير ماء _دهون الكمي يحدد توقع النسبة المئوية لكمية الدهون في كل بكسل.

المشاكل الرئيسية في وسائل تصوير ماء _دهون الحالية هي تستغرق زمن طويل لالتقاط الصورة، وأحيانا زمن إعادة تكوين الصورة طويل، وأخطاء إعادة تكوين الصورة التي تحط من جودة الصورة.

العلاقة ما بين محتويات النموذج ومحتوى الكثافة (كمية الضوء في الصورة) يمكن ملاحظتها في النموذج ذو محتوى الثلاث قنينات (الزيت، الماء، مخلوط الماء والزيت).

الرنين المغنطيسي لديه تقنيات حديثة تحتاج أن تستخدم في السودان لتطوير التشخيص والعلاج الطبي، وطريقة التطبيق وذلك بإقامة تجربة بها ثلاث قنينات يتضمن Spin echo و Advance المتقدمة وقراءة الصور الناتجة. ووجد أن الصور المستخدمة بالطرق المتقدمة أكثر وضوحاً.

وخاتمة هذه التجربة أن التشخيص الطبي يكون أكثر دقة وبالتالي يمكننا الكشف عن المرض في مراحله الابتدائية باستخدام التقنية المتقدمة لأجهزة الرنين المغنطيسي.

List of contents

List of table

List of Figure

Chapter one

1- Introduction

1-1 Definition of MRI

Unlike CT and PET, MRI does not use ionizing radiation. In addition, it has a higher spatial resolution than both modalities[1].

MRI was initially called Nuclear Magnetic Resonance Imaging after its early use for chemical analysis. The "Nuclear" was dropped off about 25 years ago because of fears that people would think there was something radioactive involved, which there is not2].

Medical MRI takes advantage of the high prevalence of hydrogen in the body and the magnetic properties of the proton in a hydrogen atom.

Hydrogen atoms induce a small magnetic field due to the spin of this atom's proton[1].

2-1 Objective:

Although magnetic resonance devices exist in Sudan and used for the purposes of medical diagnosis, but this high- potential setups only used normal margins.

The goal of this project advance technology application in Sudan for the development of medical diagnosis.

3-1 Problems Statement:

Although MR Images are more detail and powerful, but there are types of tissues that cannot distinguish between them that is, it field to compare those tissue.

A field study to see how the applications of advanced methods in the diagnosis using MRI in Sudan.

Chapter Two

2. The Basics of MRI

2.1 Introduction

Magnetic resonance imaging (MRI) is an imaging technique used primarily in medical settings to produce high quality images of the inside of the human body. MRI is based on the principles of nuclear magnetic resonance (NMR), a spectroscopic technique used by scientists to obtain microscopic chemical and physical information about molecules[3].

2.2 Microscopic Property Responsible for MRI

The human body is primarily fat and water. Fat and water have many hydrogen atoms which make the human body approximately 63% hydrogen atoms. Hydrogen nuclei have an NMR signal. For these reasons magnetic resonance imaging primarily images the NMR signal from the hydrogen nuclei[4].

2.3 Spin Physics

What is spin? Spin is a fundamental property of nature like electrical charge or mass. Spin comes in multiples of 1/2 and can be + or -. Protons, electrons, and neutrons possess spin. Individual unpaired electrons, protons, and neutrons each possesses a spin of 1/2.

In the deuterium atom (2H), with one unpaired electron, one unpaired proton, and one unpaired neutron, the total electronic spin = 1/2 and the total nuclear spin = 1.

2.4 Transitions

This particle can undergo a transition between the two energy states by the absorption of a photon. A particle in the lower energy state

absorbs a photon and ends up in the upper energy state. The energy of this photon must exactly match the energy difference between the two states. The energy, E, of a photon is related to its frequency ν by Planck's constant (h = 6.626x10-34 J s).

$$E = h\nu \_\_\_\_\_ (2, 1)$$

In NMR and MRI, the quantity is called the resonance frequency and the Larmor frequency.

2.5 Energy Level Diagrams

The energy of the two spin states can be represented by an energy level diagram[3]. We have seen that $\nu = \Upsilon B$ and $E = h\nu$, therefore the energy of the photon needed to cause a transition between the two spin states is

$$E = h \Upsilon B \_\_\_\_\_ (2, 2)$$

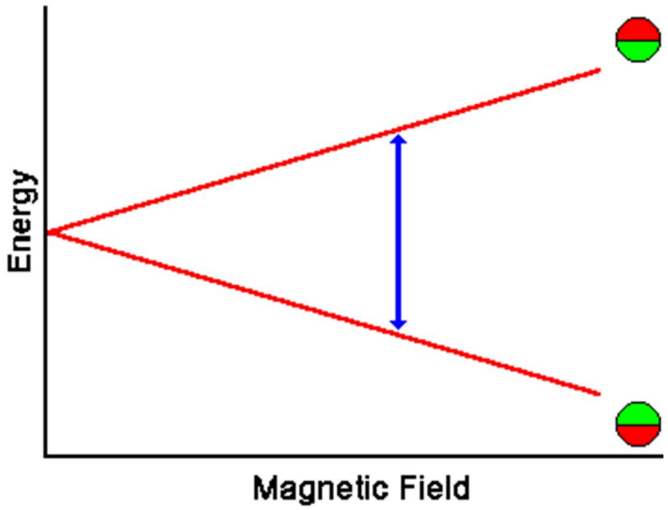

Fig (2.1) Energy Level Diagrams

2.6 T1 Processes

At equilibrium, the net magnetization vector lies along the direction of the applied magnetic field Bo and is called the equilibrium magnetization Mo. In this configuration, the Z component of magnetization MZ equals Mo. MZ is referred to as the longitudinal magnetization. There is no transverse (MX or MY) magnetization here

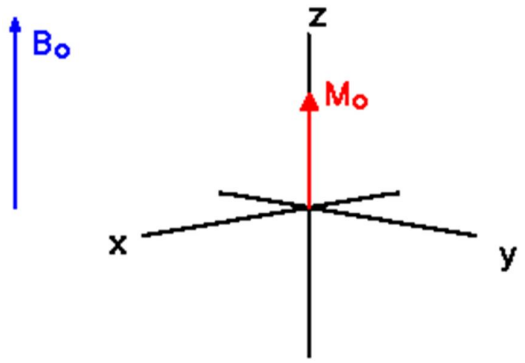

Fig (2.2) T1 Processes

It is possible to change the net magnetization by exposing the nuclear spin system to energy of a frequency equal to the energy difference between the spin states. If enough energy is put into the system, it is possible to saturate the spin system and make MZ=0

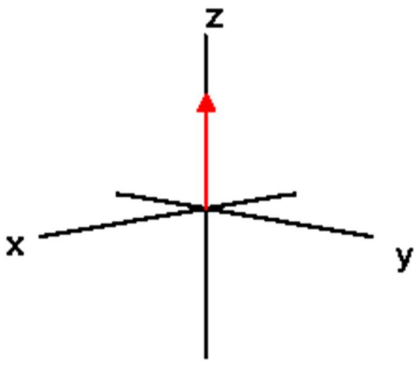

Fig (2.3) $M_z = 0$

The time constant which describes how MZ returns to its equilibrium value is called the spin lattice relaxation time (T1). The equation governing this behavior as a function of the time t after its displacement is:

$M_z = M_o(1 - e^{-t/T1})$ _____ (2, 3)

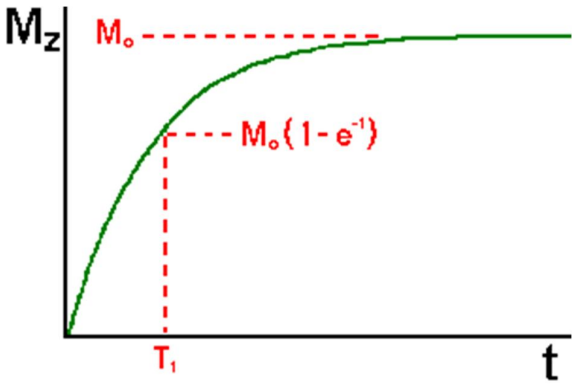

Fig (2.4) T1 Processes curve

T1 is the time to reduce the difference between the longitudinal magnetization (MZ) and its equilibrium value by a factor of e

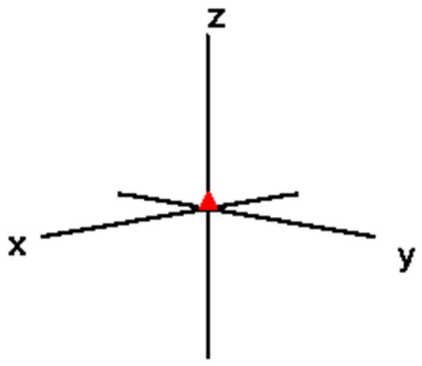

Fig (2.5) longitudinal magnetization (MZ)

If the net magnetization is placed along the -Z axis, it will gradually return to its equilibrium position along the +Z axis at a rate governed by

T1, The equation governing this behavior as a function of the time t after its displacement is:

$M_z = M_o(1 - 2e^{-t/T1})$

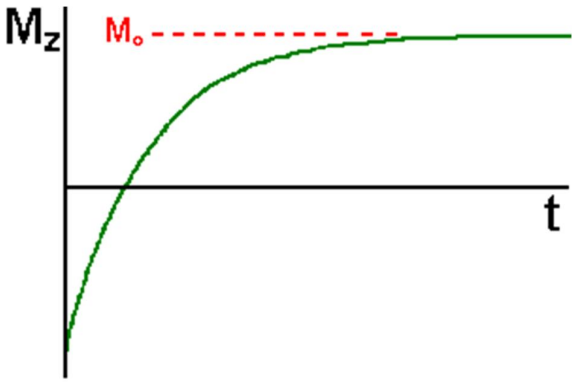

Fig (2.6) T1 equation

Again, the spin-lattice relaxation time (T1) is the time to reduce the difference between the longitudinal magnetization (MZ) and its equilibrium value by a factor of e.

2.7 Precession

If the net magnetization is placed in the XY plan

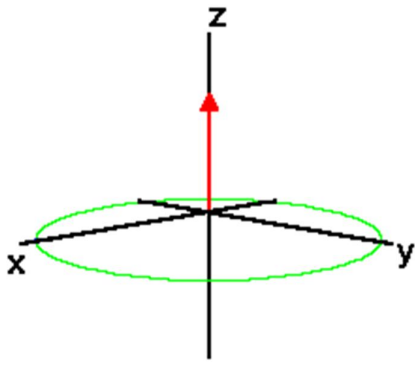

Fig (2.7) Precession

it will rotate about the Z axis at a frequency equal to the frequency of the photon which would cause a transition between the two energy levels of the spin. This frequency is called the Larmor frequency.

2.8 T2 Processes

In addition to the rotation, the net magnetization starts to de-phase because each of the spin packets making it up is experiencing a slightly different magnetic field and rotates at its own Larmor frequency.

Longer the elapsed time, the greater the phase difference. Here the net magnetization vector is initially along +Y. For this and all de-phasing examples think of this vector as the overlap of several thinner vectors from the individual spin packets

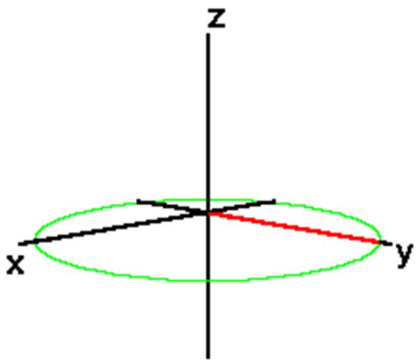

Fig (2.8) T2 Processes

The time constant which describes the return to equilibrium of the transverse magnetization, MXY, is called the spin-spin relaxation time, T2.

$$M_{XY} = M_{XY_o} e^{-t/T2} \quad \text{(2, 4)}$$

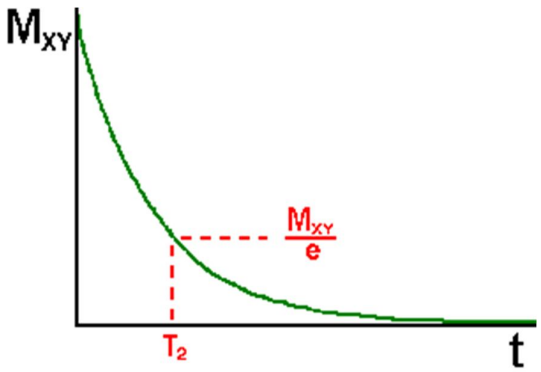

Fig (2.9) T2curve

T2 is always less than or equal to T1. The net magnetization in the XY plane goes to zero and then the longitudinal magnetization grows in until we have Mo along Z

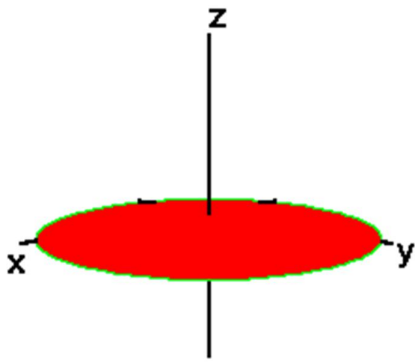

Fig (2,10) Mo along Z

Any transverse magnetization behaves the same way. The transverse component rotates about the direction of applied magnetization and de-phases. T1 governs the rate of recovery of the longitudinal magnetization.

In summary, the spin-spin relaxation time, T2, is the time to reduce the transverse magnetization by a factor of e. In the previous sequence, T2 and T1 processes are shown separately for clarity. That is, the magnetization vectors are shown filling the XY plane completely before growing back up along the Z axis. Actually, both processes occur simultaneously with the only restriction being that T2 is less than or equal to T1.

Two factors contribute to the decay of transverse magnetization.
1-molecular interactions (said to lead to a pure T2 molecular effect)
2-Variations in Bo (said to lead to an inhomogeneous T2 effect

The combination of these two factors is what actually results in the decay of transverse magnetization. The combined time constant is called T2 star

and is given the symbol T2*. The relationship between the T2 from molecular processes and that from in-homogeneities in the magnetic field is as follows:

$1/T_2^* = 1/T_2 + 1/T_{2inhomo}$. _____(2, 5)

2.9 NMR Spectroscopy

The Time Domain NMR Signal

As transverse magnetization rotates about the Z axis, it will induce a current in a coil of wire located around the X axis. Plotting current as a function of time gives a sine wave. This wave will decay with time constant T_2^*. due to de-phasing of the spin packets. This signal is called free induction decay (FID).

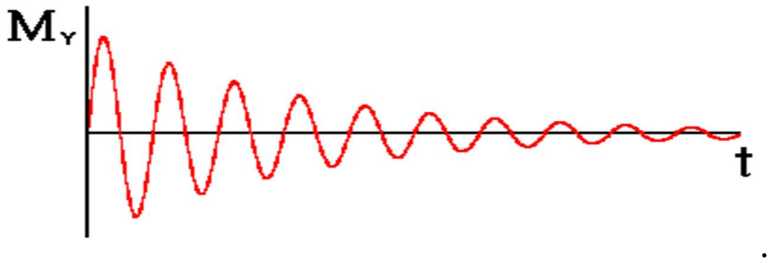

Fig (2,11) My free induction decay (FID).

2.11 Chemical Shift

When an atom is placed in a magnetic field, its electrons circulate about the direction of the applied magnetic field[4]. This circulation causes a small magnetic field at the nucleus which opposes the externally applied field.

The magnetic field at the nucleus (the effective field) is therefore generally less than the applied field by a fraction σ.

$B = B_o (1-\sigma)$ _____(2, 6)

The electron density around each nucleus in a molecule varies according to the types of nuclei and bonds in the molecule. The opposing field and therefore the effective field at each nucleus will vary. This is called the chemical shift phenomenon.

Consider the methanol molecule.

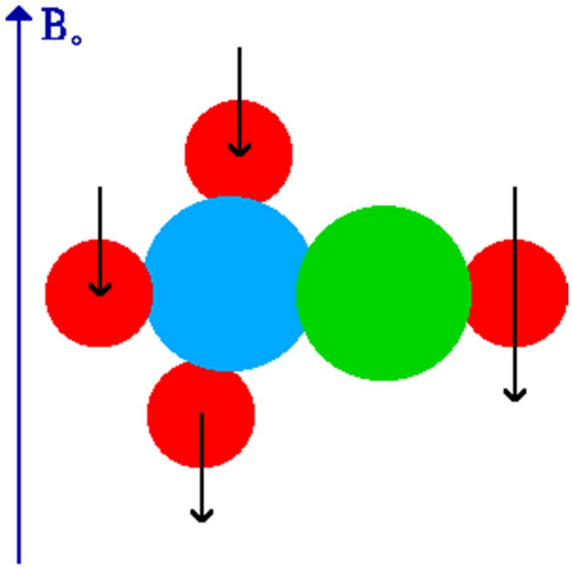

Fig (2.12) chemical shift phenomenon of the methanol molecule.

Resonance frequencies of two types nuclei in this example are differ. This difference will depend on the strength of the magnetic field, B_o, used to perform the NMR spectroscopy. The greater value of B_o, the greater the frequency difference. This relationship could make it difficult to compare NMR spectra taken on spectrometers operating at different field strengths. The term chemical shift was developed to avoid this problem.

The chemical shift of a nucleus is the difference between the resonance frequency of the nucleus and a standard, relative to the standard. This quantity is reported in ppm and given the symbol delta, d.

$$\delta = (\nu - \nu_{REF}) \times 10^6 / \nu_{REF} \quad \text{(2, 7)}$$

In NMR spectroscopy, this standard is often tetra methylsilane, abbreviated TMS. In the body there is no TMS, but there are two primary hydrogen containing substances, water and fat. The chemical shift difference between these two types of hydrogen's is approximately 3.5 ppm.

2.12 Fourier Transforms

A detailed description of the Fourier transform (FT) has waited until now, when you have a better appreciation of why it is needed. A Fourier transform is an operation which converts functions from time to frequency domains. An inverse Fourier transform (IFT) converts from the frequency domain to the time domain.

2.13 Imaging Principles

Magnetic resonance imaging is an imaging modality which is primarily used to construct pictures of the NMR signal from the hydrogen atoms in an object. In medical MRI, radiologists are most interested in looking at the NMR signal from water and fat, the major hydrogen containing components of the human body.

The principle behind all magnetic resonance imaging is the resonance equation, which shows that the resonance frequency ν of a spin is proportional to the magnetic field, B_o, it is experiencing.

$$\nu = \gamma B_o \_\_\_\_\_(2,)$$

γ is the gyromagnetic ratio.

2.14 Magnetic Field Gradient

A magnetic field gradient is a variation in the magnetic field with respect to position. A one-dimensional magnetic field gradient is a variation with

respect to one direction, while a two-dimensional gradient is a variation with respect to two. The most useful type of gradient in magnetic resonance imaging is a one- dimensional linear magnetic field gradient. A one-dimensional magnetic field gradient along the x axis in a magnetic field, B_o, indicates that the magnetic field is increasing in the x direction. Here the lengths of the vectors' represent the magnitude of the magnetic field.

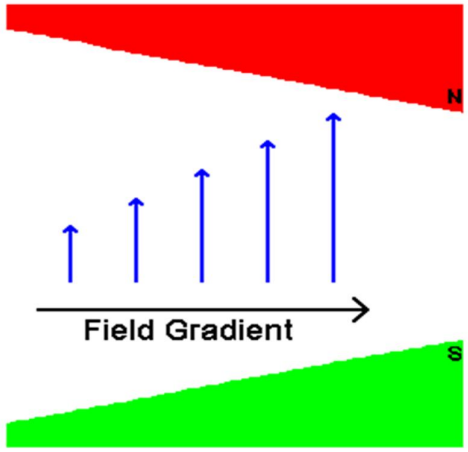

Fig (2.13) the magnitude of the magnetic field.

The symbols for a magnetic field gradient in the x, y, and z directions are G_x, G_y, and G_z.

2.15 Frequency Encoding

The point in the center of the magnet where (x,y,z) =0,0,0 is called the iso-center of the magnet. The magnetic field at the iso-center is B_o and the resonant frequency is ν_o. If a linear magnetic field gradient is applied to our hypothetical head with three spin containing regions, the three regions experience different magnetic fields. The result is an NMR spectrum with more than one signal. The amplitude of the signal is proportional to the number of spins in a plane perpendicular to the

gradient. This procedure is called frequency encoding and causes the resonance frequency to be proportional to the position of the spin.

$$\nu = \gamma (B_o + x\ G_x) = \nu_o + \gamma\ x\ G_x$$

$$x = (\nu - \nu_o) / (\gamma\ G_x)$$

2.16 Back Projection Imaging

Back projection is an extension of the frequency encoding procedure just described. In the back projection technique, the object is first placed in a magnetic field[5]. A one-dimensional field gradient is applied at several angles, and the NMR spectrum is recorded for each gradient. For example, say you wished to produce an YZ plane image of an object. A magnetic field gradient in the +Y direction is applied to the object and an NMR spectrum is recorded.

2.17 Slice Selection

Slice selection in MRI is the selection of spins in a plane through the object. The principle behind slice selection is explained by the resonance equation. Slice selection is achieved by applying a one-dimensional, linear magnetic field gradient during the period that the RF pulse is applied. A 90^o pulse applied in conjunction with a magnetic field gradient will rotate spins which are located in a slice or plane through the object. Picture what this would look like if we had a cube of small net magnetization vectors.

2.18 Imaging Hardware

MRI scanners have evolved considerably since the first commercial units were introduced in the 1980s.

The graphics window displays a schematic representation of the major systems on a magnetic resonance imager and a few of the major interconnections.

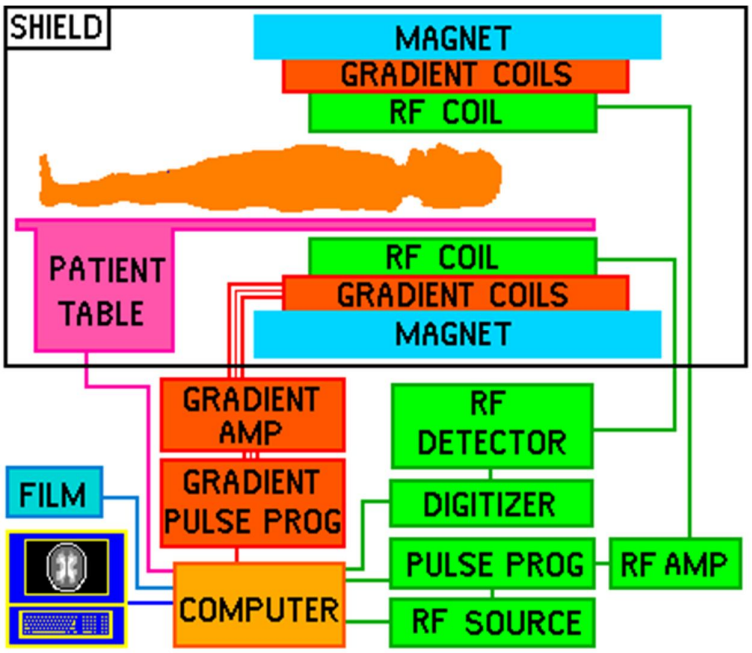

Fig (2.14) Imaging Hardware

At the top of the schematic representation you will find the components of the imager located in the scan room of a magnetic resonance imager.

2.19 Magnet

The imaging magnet is the most expensive component of the magnetic resonance imaging system. Most magnets are of the superconducting type. This is a picture of a first generation 1.5 Tesla superconducting magnet from a magnetic resonance imager. A superconducting magnet is an electromagnet made of superconducting wire.

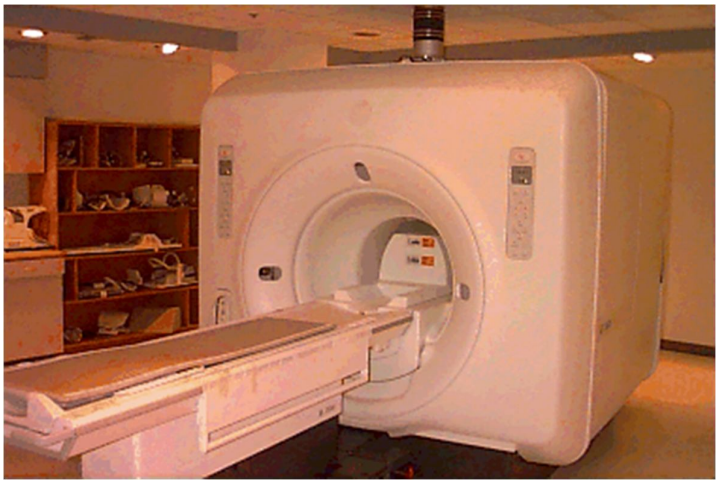

Fig (2.15) MRI Device

2.20 Gradient Coils

The gradient coils produce the gradients in the B_o magnetic field[6]. They are room temperature coils, which because of their configuration, create the desired gradient. Since the horizontal bore superconducting magnet is most common, the gradient coil system will be described for this magnet.

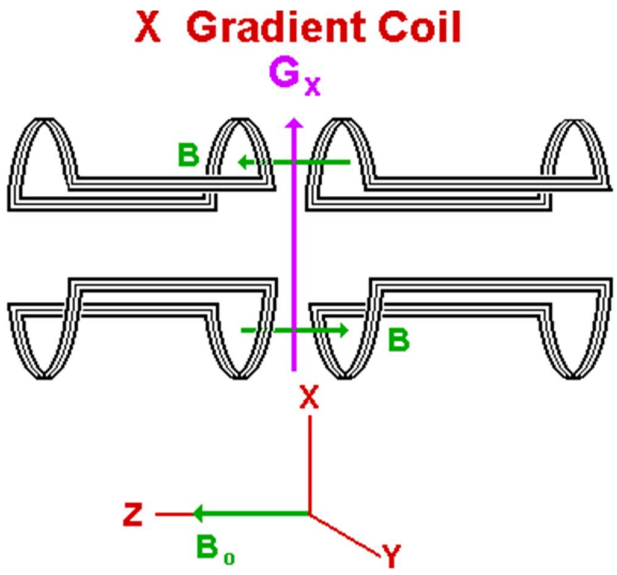

Fig (2.16) x Gradient coil

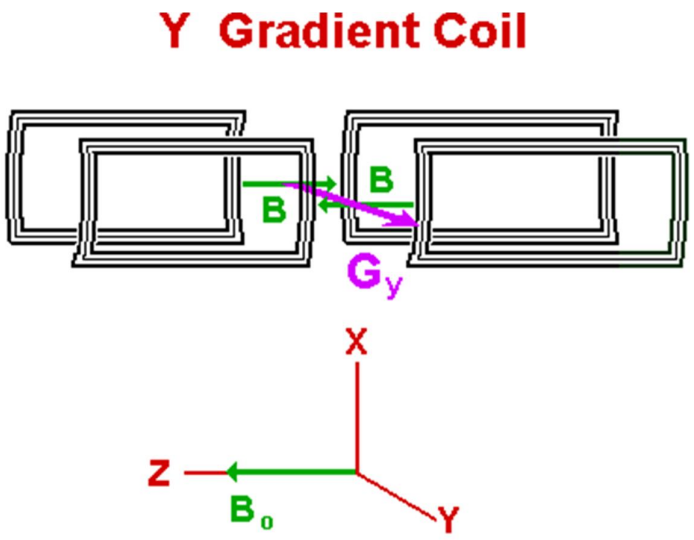

Fig (2.17) Y gradient

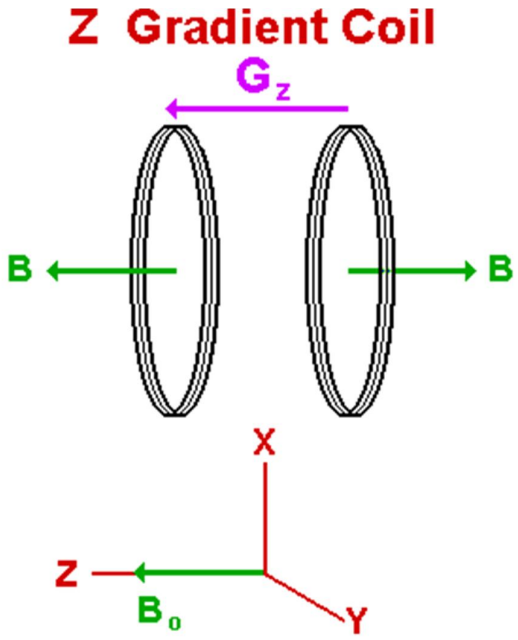

Fig (2.18) z Gradient coil

2.21 RF Coils

RF coils create the B_1 field which rotates the net magnetization in a pulse sequence. They also detect the transverse magnetization as it precesses in the XY plane.

RF coils can be divided into three general categories;

1) Transmit and receive coils,

2) Receive only coils, and

3) Transmit only coils.

2.22 RF Detector

RF detectors[7]. on MRI systems have evolved considerably since the 1980s. Initially, linear analog detectors and single channel digitizers were used. These were replaced with quadrature analog detectors with two channel digitizers. With the more recent availability of fast digitizers, single channel digitizers followed by digital quadrature detection is more common.

2.23 Safety

I am often asked, how safe is MRI? As with every piece of technology, there are risks and benefits. Those pieces of technology in wide use generally have a high benefit to risk ratio, while those with a low benefit to risk ratio are generally used more sparingly. Although MRI does not use ionizing radiation to produce images there are still some important safety considerations which one should be familiar with. These concern the use of strong magnetic fields, radio frequency energy, time varying magnetic fields, cryogenic liquids, and magnetic field gradients.

2.24 Phantom

An MRI phantom is an anthropogenic object that can be imaged to test the performance of the magnetic resonance imaging system. Phantoms are used instead of a standard human because it is much easier to locate a phantom standard at each of the many MRI systems in the world then it is

to send the standard human from site to site to be imaged. Phantoms are composed of materials that have a magnetic resonance signal. Many materials have been used as the signal bearing substance in MRI phantoms[8]. Some of these are aqueous paramagnetic solutions; pure gels of gelatin, agar, polyvinyl alcohol, silicone, polyacrylamide, or agarose; organic dapped gels; Para magnetically dapped gels; and reverse micelle solutions.

Water is most frequently used as the signal bearing substance in an MRI phantom. It is usually necessary to adjust the spin-lattice (T_1) and spin-spin (T_2) relaxation times of aqueous solutions so images may be acquired in reasonable time periods (i.e. short TR). Paramagnetic metal ions are typically used to adjust the relaxation times of the water hydrogen's. The approximate functional form of the T_1 and T_2 values of aqueous solutions of various paramagnetic species at 1.5 T are listed below.

2.24.1 Aqueous Nickel

$T_1(s) = 1/(632\ [Ni\ (mole/L)] + 0.337)$

$T_2(s) = 1/(691\ [Ni\ (mole/L)] + 1.133)$

Nickel in 10 wt. % gelatin

$T_1(s) = 1/(732\ [Ni\ (mole/L)] + 0.817)$

$T_2(s) = 1/(892\ [Ni\ (mole/L)] + 4.635)$

2.24.2 Aqueous Oxygen

$T_1(s) = 1/(0.013465\ [O_2\ (mg/L)] + 0.232357)$

2.24.3Aqueous Manganese

$T_1(s) = 1/(5722\ [Mn\ (mole/L)] + 0.0846)$

$T_2(s) = 1/(60386\ [Mn\ (mole/L)] + 3.644)$

2.24.4 Aqueous Copper

$T_1(s) = 1/(606\ [Cu\ (mole/L)] + 0.349)$

$T_2(s) = 1/(850\ [Cu\ (mole/L)] + 0.0357)$

Here are four basic types of MRI phantoms: resolution, linearity, homogeneity, and signal. The latter is used to affirm the signal or some measurable property from the signal that results from a pulse sequence. Examples of this type are a T_1 phantom and a diffusion coefficient phantom. Homogeneity phantoms can be used to measure both the RF and B_o homogeneity. Resolution, linearity, and homogeneity can be used to measure the B_o homogeneity, but they allow the measurement of homogeneity to be made differently than in the homogeneity phantom. The following paragraphs describe the differences in more detail.

2.24.5 Resolution and Linearity Phantoms

A resolution and linearity phantom can be used to test several spatial properties of an imager. These spatial properties include in-plane resolution, slice thickness, linearity, and the signal-to-noise ratio as a function of position. Resolution phantoms are typically constructed from plastic. Portions of the inside of the phantom are removed to create a test pattern. The phantom is filled with an aqueous solution. When imaged, the image displays the signal from the water in the removed portions of the plastic. Some resolution phantoms also have signal standards with known T_1, T_2, and ρ values that allow the phantom to be used to test contrast-to-noise ratios.

Here is an example of a resolution phantom.

Fig (2.19) resolution phantom

2.24.6 Homogeneity Phantoms

Homogeneity phantoms are used to test the spatial uniformity of the static magnetic field, as well as transmit and receive radio frequency magnetic fields. Let us first address their use for monitoring the homogeneity of the B_o magnetic field.

The NMR spectral line width (Γ) of a single spin packet equals

$$\Gamma = (\pi\, T_2)^{-1}.$$

Because thereby definition a uniform applied magnetic field. As the volume of the signal bearing material increases, the line width becomes

$$\Gamma = (\pi\, T_2^*)^{-1}.$$

Because the magnetic field varies from location to location r. The smaller this variation made smaller distortion in the image. A high resolution NMR spectrometer can have a line width of 0.5 Hz for sample in a 5 mm NMR tube. In a clinical imager, the variation in B_o across a 27 cm diameter spherical phantom filled with water causes the NMR line width from the phantom to be 30 to 40 Hz. This is because there is a broad distribution of resonance frequencies for all the spin packets in the sample. The width of absorption line for a large volume phantom is therefore a measure of the distribution of magnetic field values across the volume of the phantom.

Homogeneity phantoms are also used to test the spatial uniformity of transmits and receives radio frequency magnetic fields. The transmit RF field (B_{1T}) is the B_1 field is that used to rotate magnetization. The receive RF field (B_{1R}) is the sensitivity of the RF coil to signals from precessing spin packets. The ideal situation for most transmit/receive coils is a spatially uniform B_{1T} to assure uniform rotation of the spins, and a spatially uniform B_{1R} to assure uniform sensitivity across the imaged object. Here is a picture of a 27 cm diameter homogeneity phantom.

Fig (2.20) homogeneity phantom

2.24.7 Diffusion Phantoms

Diffusion phantoms are phantoms which can be used to test the performance of a diffusion imaging sequence. Some consist of vials of liquids with different diffusion coefficients[9].

Since the solution is isotropic, the phantom will yield the same diffusion coefficient in x, y, and z. Geometrical diffusion phantoms rely on special geometries to create anisotropic diffusion. For example, a set of parallel tubes will have unrestricted diffusion along the axis of the tube, and restricted diffusion along a diameter of the tube. Parallel plates will have unrestricted diffusion parallel to the plates, and restricted diffusion perpendicular to the plates. One diffusion phantom contains hydrated parallel fibers[10].

2.24.8 Fat-Saturation Phantoms

Fat saturation phantoms consist of liquids with two chemical shifts, one for water and one for fat. These are usually oil-water emulsions. Since body fat contains multiple peaks, better fat saturation phantoms contain oils with multiple peaks similar to body fat[11].

2.24.9 T_1 and T_2 Phantoms

T_1 and T_2 phantoms contain liquids with specific T_1 and T_2 values. These liquids are usually aqueous solutions of paramagnetic materials.

Chapter three

3. Previous Studies

3.1Advanced MR technique development for improved characterization of multiple sclerosis (Metcalf et al 2008)

Magnetic resonance imaging (MRI) provides many ways to study human brain anatomy as well as advance our understanding of brain structure, function, and processes that occur with disease. This dissertation project investigated the clinical utility of new and existing MRI techniques to the study of changes that occur in the brains of patients with multiple sclerosis (MS). The new MRI techniques were developed and tested with the goal of attaining more sensitive methods for disease detection than those that are currently available to clinician scientists. These new bioengineering developments included both novel MR acquisition and data analysis techniques for improved non-invasive, quantitative assessments of multiple sclerosis disease processes.

There are many quantitative MRI methods that can be used to detect tissue differences in patient populations when compared to controls. This dissertation research probed the utility of volumetric measurements, T1-relaxation times, and diffusion tensor imaging (DTI) metrics to detection of tissue damage and disease in early stage MS.

It was determined that T1-relaxation and DTI measures of mean diffusivity (Dav), fractional anisotropy (FA), and transverse diffusion (EvT) were sensitive enough to detect brain tissue changes at the earliest presentation of disease. Although volume measurements were not different as a group at presentation, atrophy was detectable via volumetry at one-year post baseline. Additionally, DTI measures were able to predict this change, an indication of a causal relationship between microscopic damage and overall tissue loss. The diffusion technique

development and high field MRI methods demonstrated the feasibility to collect images with advantages in image quality, signal to noise (SNR), resolution, and ability to detect disease over what was previously available. These developments provide the platform for future work in MRI and its application in MS to better characterize disease[12].

3.2Implementation Of Dixon Methods For Preclinical Mr Imaging At High Fields Radim 2015:

Preclinical magnetic resonance (MR) imaging in small animals is a very popular procedure that requires a higher sensitivity, given the small size of the subjects. A higher sensitivity can be reached when an MR imaging system with a high magnetic field is used (e.g., 4.7 T or higher). The benefits of such sensitivity include, for example, a higher resolution, an improved signal-to-noise ratio (SNR), an increased chemical shift, and a longer $T1$ longitudinal relaxation time. On the other hand, a high field causes stronger static magnetic field deformation along the borders between tissues with different susceptibilities, and it also results in the shortening of the $T2$ transversal relaxation. Adipose tissue is significantly contained in the human (or mammal) body and is primarily used to store energy in the form of fat. This tissue can be classified into white and brown subsets. Brown adipose tissue is found mainly in new-born children, and a certain (yet very small) amount of such tissue can be traced also in adults. White adipose tissue then ensures the storage of fat as a source of energy. Furthermore, white adipose tissue produces adipokines, hormones, and many other substances important for metabolism. Generally, fat can be regarded as a biomarker in the case of specific diseases (obesity, steatosis – fatty liver disease, and others). Thus, the quantification of fat is a precondition for correct diagnosis. MR imaging comprises a special group of methods for water-fat separation; these methods are referred to as Dixon methods and utilize the principle of chemical shift. In this thesis, a new $T2$ – weighted sequence for Dixon acquisition is introduced (Chapter 4). The proposed sequence is a very time-effective three-point (3PD) method. The newly proposed sequence of fast triple spin echo Dixon (FTSED) is derived from the original fast spin echo sequence (FSE). Such modification of the original FSE sequence leads to a novel FTSED sequence, where three images are

acquired simultaneously without any increase of the total acquisition time. The discussed sequence was successfully implemented on a 9.4 T MR imaging system at the Institute of Scientific Instruments, ASCR Brno. The acquired data were calculated through the use of the IDEAL (iterative decomposition of water and fat with echo asymmetry and least-squares estimation) algorithm. The results of the computation are water and fat images, and the fat fraction (FF) can be calculated from these. The sequence was successfully tested in a rat. The successful FTSED implementation on a 9.4 T MR imaging system enables this method to be used in low-field MR imaging systems[13].

3.3 MRI in the Prediction and Diagnosis of Pediatric Onset MultipleSclerosis: Insights from Children with Incid ent CNS Demyelination Leonard Herman Verhey,2012:

An acute demyelinating syndrome (ADS) in a child may be a monophasic illness or may represent the incident attack of multiple sclerosis (MS) – an inflammatory demyelinating neurodegenerative disorder affecting the brain, spinal cord and optic nerves. The central objective of this dissertation was to identify MRI parameters present at ADS that predict MS diagnosis. A scoring tool was first created containing 14 parameters identified from the literature and demonstrating substantial inter-rater agreement (Cohen's kappa values ≥0.6).

Children aged <16 years were enrolled at incident ADS and are currently followed for five years at 23 Canadian centers. Standardized MRI scans were acquired at onset and serially. MS was defined based on the occurrence of a second demyelinating attack or MRI evidence of new lesions in accordance with McDonald criteria for dissemination in time. Multivariable Cox proportional hazards regression models were used to identify MRI parameters that predicted MS diagnosis. Over 1100 MRI scans in 284 children with ADS were evaluated. To date, 57(20%) children have been diagnosed with MS. For those that developed MS, the median (IQR) time from incident attack to diagnosis was 6.2 (4.7-11.1) months. The presence of ≥1 T1-hypointense lesion (HR 20.6, 95% CI 5.5-78.0) and ≥1 T2 periventricular lesion (3.3, 1.3-8.8) were associated with an increased likelihood for MS diagnosis (sensitivity 84%, specificity 93%, PPV 76%, NPV 96%). The predictive parameters were validated in an independent Dutch cohort of 45 children with ADS (n=15,

33% MS): sensitivity 93%, specificity 87%, PPV 78%, NPV 96%. Finally, it was determined that the 2010 McDonald criteria are applicable for diagnosis of pediatric-onset MS diagnosis in older children with non-ADEM presentations. The work embodied herein emphasizes the value of MRI in predicting MS diagnosis in children with incident ADS.

Early identification of children with MS is important for planning clinical care and will be valuable in future pediatric MS treatment trials[14].

3.4 Quantification of Fat Content and Fatty Acid Composition Using Magnetic Resonance Imaging Pernilla Peterson,2013:

In obesity and several other disease scenarios, the measurement of fat accumulation in various organs and tissues has become a sought-after technique in clinical diagnostics and research. Especially, quantitative and non-invasive techniques which also provide images of accumulated fat throughout the body would be valuable. In the typical hospital, magnetic resonance imaging (MRI) is the only technique available which has the potential for these types of measurements and out of techniques suggested, Water/Fat Imaging is particularly promising. Water/Fat Imaging is based on the separation of water and fat, the two main contributors to the MRI signal, with the use of the frequency separation between their signals. The field has inspired a wide range of research and is by now well established, especially for investigations of fatty liver.

However, in this and several other applications there is a continued need for method development. The fat concentrations in skeletal muscle are expected to be very low. Thus, for this application, there is an increased demand for measurement precision. The results presented in this thesis indicate that fat concentrations below 1 % are possible to measure using Water/Fat Imaging. In addition, precision may be increased using a higher flip angle if a pure fat reference is used for quantification, without compromising quantification accuracy. (Papers I and II) Water/Fat Imaging has become an appreciated technique for abdominal applications in which breath-hold is necessary for acceptable image quality. The use of a bipolar acquisition scheme may be used to reduce the total scan time, but is associated with issues which are detrimental to fat quantification. Using a built-in correction approach, it is demonstrated that accurate and

noise efficient fat quantification is possible using a bipolar acquisition. (Paper III) The basic ideas of Water/Fat Imaging may be extended to not only quantify the fat concentration, but also the fatty acid composition. In this thesis, a reconstruction algorithm is suggested and its accuracy is demonstrated in a wide range of fat concentrations and fatty acid compositions. In addition, a number of potential sources of bias are investigated. Out of these, accurate modeling of the individual T2 values of fat and water is especially important in fat/water mixtures, whereas some T1 weighting may be allowed with small impact on quantification accuracy[15].

Chapter four

4. Fat suppression

4.1 Chemical shift

4.1.1 Introduction:

Shortly after the first observation of the NMR phenomenon, physicists discovered that all protons didn't exhibit exactly the same Larmor frequency when submitted to the same external magnetic field. For instance, if hydrogen nuclei of hydrocarbon resonate at 40MHz, the hydrogen nuclei of water would be characterized by a Larmor frequency that differs from the hydrocarbons by approximately 10 Hertz. Since it was difficult to explain these differences by variations in the magnetogyric ratio, the origin of the phenomenon was attributed to local variations of external field B_o.

The frequency shift experienced by a given kind of proton depends on the external field strength through a refined form of the Larmor frequency which includes the 'screening effect'

$\text{Ƒ} = \text{gamma}.\ (1\text{-sigma}).\ B_o$ _____(4, 1).

Gamma is the magnetogyric ratio (42,575,900 Hz/T for ^1H) and sigma is called the screen constant.

The frequency different between –CH2- and H2O in muscles observed at 1T is 142Hz. This difference will be 284Hz at 2 T.

Chemical shift between two peaks is defined as the distance between a reference peak and the peak under study. The distance is measured in parts per million (ppm) with respect to a reference. In the case of muscle, if we suppose that a reference compound is resonating compound is resonating at 42,575,900 Hz, the chemical shifts are:

CH2 :($\frac{42{,}575{,}955-42{,}575{,}900}{42{,}575{,}900}$ = 1.3 ppm_____(4, 1, 2)

H2O: $\frac{42{,}575{,}100-42{,}575{,}900}{42{,}575{,}900}$ = 4.6ppm_____(4, 1, 3)

Note that if the chemical shifts are measured in ppm, then they are dependent on the field strength[16].

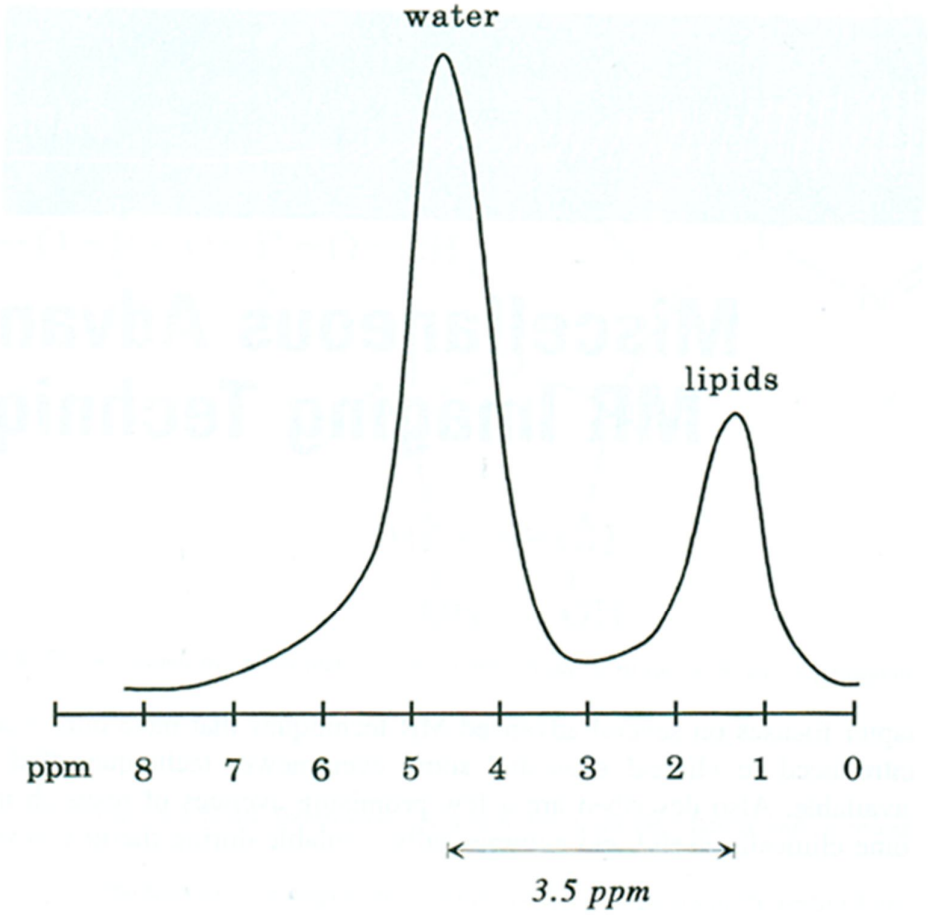

Fig (4.1) Chemical shift graph between water and lipids[17]

4.2 Techniques of Fat Suppression

The Magnetic Resonance (MR) signal used to create MR images is induced by hydrogen nuclei. All hydrogen nuclei in the object being imaged (i.e. the subject) contribute to the MR signal but for many of these nuclei (e.g. hydrogen nuclei on fatty acid chains in cell membranes)

their contribution decays too quickly to contribute to the measured signal. The actual signal is composed mainly of contributions from hydrogen nuclei residing on water molecules and fat molecules in adipose tissue. In this article these hydrogen nuclei will be referred to as “water spins” and “fat spins”, respectively. The net effect of these spin groups are an induced effective magnetic field or magnetization. The magnetization for these groups will be referred to here as water magnetization and fat magnetization, respectively. The signal generated by each of these magnetizations will be referred to as water and fat signals, respectively.

There are many situations in clinical MRI where it is desirable to remove the fat contribution from the total MR signal without affecting the water signal. Fat suppression techniques can be used to enhance tissue contrast and lesion conspicuity, to determine if the tissue of interest has high or low lipid content and to remove artifacts. Specific examples include suppression of the marrow signal from around joints and in vertebrae and the suppression of the fat signal in the orbits to better differentiate tissues of interest (cartilage and ligaments, bone metastases, optic nerve, etc.) from surrounding fatty tissue. Suppression of hyper intense fat signals may also be useful in post contrast images where lesions may appear bright.

To suppress the fat signal for a given MR sequence a fat suppression module is typically inserted at the beginning of an otherwise normal MRI sequence. To prepare the signal such that the fat contribution is as small as possible, without perturbing the water signal, one or more of the following properties is exploited:

1. Fat and water have different resonant frequencies,
2. They have different Larmor Precession frequencies and

3. They have different T1 relaxation time

The water signal has identical contributions from its two hydrogen atoms. Fat signals can have contributions from many in equivalent hydrogen atoms (e.g. CH3, CH2, CH=CH, etc.) each of which will have distinct resonance frequencies. The most important fat resonance peaks occur at frequencies between 3.3 and 3.5 ppm lower than the water resonance peak. The signal from the CH2 groups in the aliphatic chain gives the strongest peak and it occurs 3.35 ppm lower than water [18], which corresponds to a frequency of 214 Hz lower than the water resonance frequency at 1.5 T and 428 Hz lower at 3.0 T.

A number of quite different fat suppression techniques are available, each with its own advantages and disadvantages. The rest of this article provides of an explanation of the following fat suppression techniques: 1) Spectral Fat Saturation, 2) STIR, 3) SPIR, 4) the Dixon method and 5) water excitation.

Fat saturation

Fat saturation is also known as FATSAT or CHESS. In contrast to STIR, fat saturation techniques rely on the molecule-specific chemical shift of fat.

It is assumed that all fat protons are chemically shifted approximately

1.3 ppm, i.e. the chemical shift of the fat bulk methylene protons (resonance B in fig. 3.4). Fat saturation is achieved by applying a selective 90◦ saturation pulse, tuned to the methylene resonance frequency, before proceeding with a nonselective excitation pulse [19]. The saturation pulse is amplitude modulated to obtain a narrowband frequency response centered around 1.3 ppm, in order not to saturate the

water protons, which precess faster and have a chemical shift of 4.7 ppm. After the saturation pulse, a gradient may be applied to spoil the transversal magnetization of the fat protons [20, 21].

In particular, this is necessary if the excitation pulse is smaller than 90◦. Fat saturation can be added to most pulse sequences. In general, narrowband pulses have long duration. Typically, some milliseconds are added to the TR.

Unlike STIR, fat saturation can be combined with the use of contrast agents. The main disadvantage is the sensitivity to B0 inhomogeneity, which causes resonance frequency shifts of all protons. This may result in local failure of the fat suppression or even inadvertent suppression of water signal. At higher field strengths, inhomogeneity of the rotating B1 field may also be a problem. This can be avoided by using of adiabatic pulses, which are amplitude- and frequency modulated pulses insensitive to B1 inhomogeneity [22].

Even if fat saturation is specific to protons in fat, not all fat signal can be

suppressed. For instance, olefin protons (−CH = CH−; resonance J in fig.(4.2) have a chemical shift of ≈ 5.3, close to that of water protons [2].

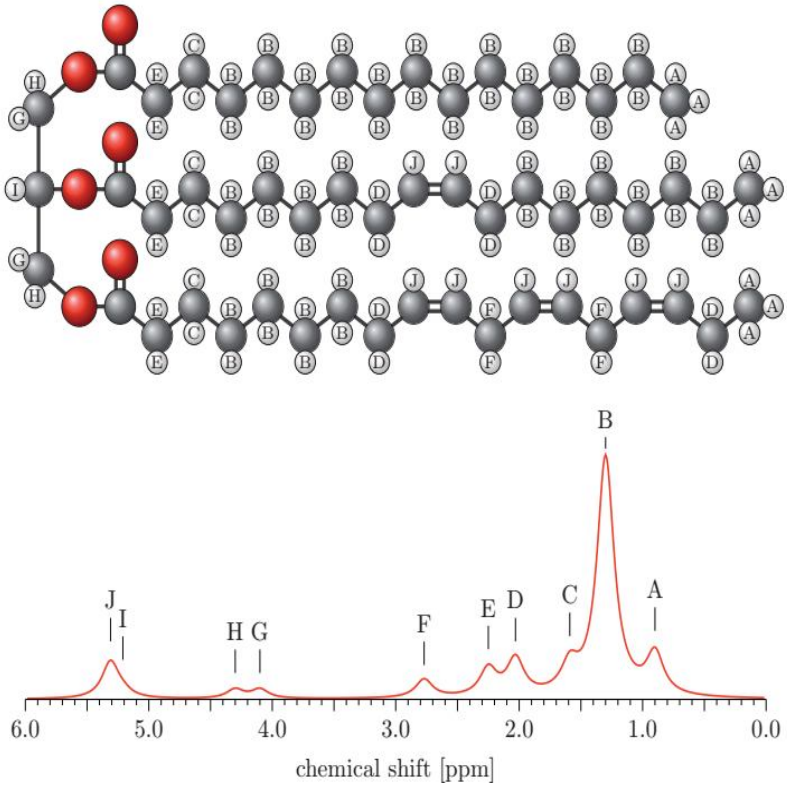

fig.(4.2) olefin protons saturation

Spectral Fat Saturation:

With this form of fat suppression the fat resonance is excited selectively and then the signal is “spoiled” using gradient pulses. The fat spins are initially tipped into the transverse plane using a special 90° pulse that affects only the fat spins. After the RF pulse, the fat spins are aligned perpendicular to the main magnetic field, B0, while the water spins are still parallel to B0. If a signal were to be measured at this point it would have contributions from fat spins only. However, spoiler gradient pulses are used to diphase the fat spins causing the fat signal to decay to zero without affecting the water spins, which are still in equilibrium. At this point, the fat signal is said to be “saturated”. The fat signal has been

suppressed and a standard MR sequence can now be initiated. The resulting image should, in principle, have no contribution from fat spins.

In order to take advantage of the different resonant frequencies for fat and water molecules, the overlap of their spectral peaks must be as small as possible. This involves both maximizing the frequency difference between the peaks and minimizing the spread of the peaks. The main fat resonance peak is at a frequency which is lower than the water resonance frequency by 3.35 ppm [18](i.e. 214 Hz at 1.5 t and 428 Hz at 3.0 T). As the magnetic field increases the frequency difference between the two resonances also increases. Consequently, fat suppression techniques based on this property tend to work better at higher magnetic field strengths. The width of the peaks should, in principle, be a reflection of the distribution of magnetic environments inherent to the subject.

However, the observed distribution of resonance frequencies, as given by the width of the measured resonance peak, may be dominated by in homogeneities of the applied magnetic field rather than the magnetic field distribution inherent to the subject, although both contribute. On low field systems or poorly shimmed magnets the width of the resonance peaks may be large compared to their separation resulting in substantial overlap of the fat and water resonance peaks. Under these conditions, fat saturation does not suppress the fat signal very well. Spectral fat saturation does not work well on low field systems or poorly shimmed magnets. Conversely, at high fields and/or on well shimmed magnets the fat and water resonance peaks do not overlap, leading to good fat saturation. The homogeneity of the magnetic field, and therefore the quality of the fat suppression, is normally also better near the iso-Centre of the magnet.

The RF pulse used in Spectral Fat Saturation must be designed to excite only fat spins. The central frequency of the RF excitation must be lower than the water resonance frequency by 3.35 ppm (214 Hz at 1.5 T and 418 Hz at 3.0 T). The frequency range excited, or spectral bandwidth (not to be confused with readout bandwidth), must also be carefully selected so that only fat spins are excited. Note that both the central frequency offset relative to the water resonance frequency and the spectral band width of the fat excitation pulse change with the magnetic field strength used. The quality of the fat saturation also deteriorates if the flip angle of the rf pulse is different at different positions in the subject unless an adiabatic spectrally selective RF pulse is used. Adiabatic pulses are specifically designed to be insensitive to RF spatial no uniformity.

For sequences with multiple repetitions (e.g. a conventional spin echo or gradient echo sequence) the fat suppression must typically be applied before each repetition, unless TR << T1fat, as may be the case with some gradient echo sequences. To compensate for regrowth of the fat signal during the sequence a tip angle greater than 90° can sometimes be used for the initial fat excitation pulse.

STIR (**S**hort **T**I **I**nversion **R**ecovery or **S**hort **T**au **I**nversion **R**ecovery):

STIR is an inversion recovery sequence where the value of the inversion time, TI, is chosen such that the fat signal does not contribute to the resulting image [23]. With this fat suppression technique the total signal (fat and water) is initially inverted (i.e. flip angle = 180°) and allowed to relax back to equilibrium via T1 relaxation. The inversion RF pulse causes spins initially parallel to the main field to become oriented anti-parallel to the main field (i.e. the initial magnetization, **M0**, becomes – **M0**). As the spins relax back to their equilibrium configuration (with the

magnetization parallel to the main field) the signal for each spin group will evolve from a negative signal, through zero (i.e. the null point), to a positive signal, at a rate which is determined by the T1 of the spin group. Since at 1.5 T, T1fat = 260 ms [24] and for most other tissues T1 ≥ 500 ms [22], the null point for the fat signal will occur much sooner than for other tissues. The actual T1 values vary with magnetic field strength but this general trend is maintained. At the fat null point the fat signal will be zero but the signal for the other tissues will normally be non-zero. Therefore, if a standard MRI sequence is started when the fat signal is at its null point then the fat spins will not contribute to the resulting image.

In principle, the fat null point will be reached when TI = T1fat*ln2 = (260 ms)*0.693 = 180 ms at 1.5 T [25].

In practice, the optimal value will also depend on other sequence parameter settings (e.g. TR); typically

TI is chosen to be less than the theoretical null point (e.g. 150 ms at 1.5 T). TI will also depend on field strength since T1fat increases with field strength.

Since STIR is an IR technique, the resulting fat suppressed image will be inherently T1-weighted; however, the T1-contrast will be inverted (unless signal phase is considered) relative to conventional T1-weighting: tissues with a short T1 will appear dark while tissues with a long T1 will be bright. All signals will relax during the TI period so the resulting tissue signals will be smaller by the amount these tissues relax during this time. For example, if TI = 180 ms and T1tissue = 700 ms then the magnitude of the tissue magnetization at TI (i.e. the start of the image acquisition) will be |-0.55M0| or 55% of its full value. T1fatis normally much shorter than the T1 of other tissues but this is not always the case (e.g. sub-acute

hemorrhage). When T1fat≈T1tissue the signal from that tissue will also be substantially suppressed when

STIR fat suppression is used. T2-weighting can also be introduced, if desired, by using a moderate to long TE. The T2 contrast is not inverted.

One disadvantage of STIR is its relatively long acquisition time, even with interleaved IR, since TR must be longer than for conventional T1-weighted acquisitions to give the spins enough time to recover. STIR is also sensitive to spatial non uniformity of the applied RF pulse (unless an adiabatic rf pulse is used). If the strength of the RF pulse varies from one position to another within the subject then the tip angle of the inversion pulse, and the quality of the fat suppression, will also vary with position. However, STIR is insensitive to inhomogeneity of the main static magnetic field, B0. Unlike spectral fat saturation, STIR works well even on low field systems and poorly shimmed magnets.

SPIR (Spectral Pre-saturation with Inversion Recovery):

SPIR is a fat suppression technique that makes use of both selective excitation of the fat signal and T1relaxation. As with STIR, an inversion rf pulse is used, but unlike STIR, this pulse is designed to excite only the fat spins. This is similar to the situation with Spectral Fat Saturation except that the spectrally selective RF pulse in STIR is an inversion pulse which causes the fat magnetization to tip through 180° (i.e. to be anti-parallel to the main magnetic field) without affecting the water signal. After the inversion, the fat spins evolve back to their equilibrium orientation parallel to the main field. As they pass through the fat null point (i.e. when the fat signal is zero) a conventional MR sequence is initiated.

The resulting image will be fat suppressed. The TI value at which fat is nulled will, in principle, be the same as for STIR; however, when other sequence parameters are considered the optimal setting may be different.

Although the implementation of STIR and SPIR may seem similar the resulting images are significantly different. SPIR has several important advantages over STIR. SPIR fat suppression does not cause inherent T1-weighting since the water spins are not affected (i.e. inverted) by the fat suppression procedure. The MR sequence that follows the fat suppression module can, in principle, be any conventional MR sequence. If the acquisition parameters for this sequence are set to create T1-weighting, the contrast is not inverted as it would be with a STIR sequence. SPIR also has inherently higher pixel intensities than STIR for tissues that do not contain fat. Furthermore, signals from tissues

with T1 values that are close to that of fat, such as contrast enhanced tissues, will not be suppressed, as they would be with STIR.

Disadvantages of SPIR are that 1) it requires good separation of the fat and water resonance peaks 2) it is sensitive to RF pulse spatial non uniformity (i.e. flip angle changing with position) and 3) it lengthens the exam time significantly relative to a similar acquisition without fat suppression. On low field systems or poorly shimmed magnets the fat and water resonances may overlap making it impossible for the spectrally selective RF pulse to excite only fat spins. SPIR also requires that the inversion pulse be the same for all fat spins in the slice. If the intensity of the RF pulse varies spatially (i.e. poor B1 uniformity)there will be a range of tip angles and fat suppression will be better in some parts of the image than in others. Sometimes SPIR is implemented with an adiabatic spectrally selective pulse.

When this is the case, the SPIR fat suppression module is not sensitive to B1 non uniformity since adiabatic pulses are specifically designed to be insensitive to B1 non uniformity.

The Dixon Method:

The principle upon which the 2-point Dixon technique [26,27] is based is that, since fat and water have different resonance frequencies, they will also process in the transverse plane at different rates (i.e. they have different Larmor precession frequencies). By adjusting the sequence timing, the phase of the fat spins relative to the water spins in the transverse plane can be adjusted to whatever phase angle is desired when the signal is acquired. In the 2-point Dixon method two images are acquired; one with the fat and water spins in-phase and the other with them out-of-phase. These images can be obtained from separate acquisitions or as different echoes of the same acquisition. If these two images are added together pixel by pixel the result will be a fat suppressed image. Conversely, if these images are subtracted the resulting image will be water suppressed. Note that the complex pixel intensities must be used for these calculations. If only the pixel magnitudes are used the resulting images will be incorrect when the fat signal coming from the voxel is stronger than the water signal.

The phase difference between the water and fat spins in the transverse plane following an RF excitation pulse is given by $\Delta\theta = 2\pi\Delta f*TE$ where Δf is the difference in their resonance frequencies (in Hz) and TE is the echo time (in seconds). From this equation it can easily be shown that $\Delta\theta = n\pi$ (i.e. the in and out of phase conditions) when TE = 2.30n ms for n = 0, 1, 2, ... , since Δf= 217 Hz at 1.5 T. Similarly, at 3T it can be shown that $\Delta\theta = n\pi$ when TE = 1.15n ms for n = 0, 1, 2,... It is necessary to have

good gradient hardware at 3T in order to achieve a double gradient echo with TE's of 1.15 ms (out-of-phase) and 2.30 ms (in-phase).

The discussion given in the previous paragraph applies to gradient echo sequences. The situation with spin echo sequences are slightly more complicated since there is both an excitation (90°) pulse and are focusing (180°) pulse. The refocusing pulse acts to undo the de-phasing that occurs between the two pulses such that the fat and water spins are in-phase again at $t = 2\tau$, where τ is the time between the 90°and 180° pulses. In this case, $\Delta\theta = 2\pi\Delta f^*(TE - 2\tau)$, from which it can be shown that, for a spin echo sequence, $\Delta\theta = n\pi$ when $TE - 2\tau = 2.30n$ ms for $n = 0, \pm1, \pm2, \ldots$, at 1.5 T and $\Delta\theta = n\pi$ when $TE - 2\tau = 1.15n$ ms for $n = 0, \pm1, \pm2, \ldots$ at 3.0 T.

The 2-point Dixon method assumes that the phases of the fat and water spin in the transverse plane are determined exclusively by the applied magnetic field, B0. B0 inhomogeneity or other effects that could affect the phase (e.g. susceptibility variations and eddy currents) are ignored. Normally these effects are not important but, for cases where they cannot be neglected, the 3-point Dixon method [29] can be used. The 3-point Dixon method is very similar to the 2-point Dixon method except that an extra image is required. Typically, images with $\Delta\theta = 0$, π, and 2π will be obtained. The first two corresponds to the images used in the 2-point Dixon method and the third is used to correct for miscellaneous phase errors. The $\Delta\theta = 0$ and 2π signals should have the same phase behavior and any deviation from this will be due to B0 inhomogeneity, susceptibility variations, eddy current effects, etc. The phase error can be determined from these two images and the correction applied to the $\Delta\theta = 0$ and π images. These corrected in-phase and out-of-phase complex

images are then added and/or subtracted to get fat and/or water suppressed images, respectively.

One disadvantage of the Dixon methods on some systems may be increased exam time since two (or more) images are required. However, these images can normally be acquired at the same time using a two (or more) echo sequence. Another disadvantage of the sequence is that the TE values used are normally quite short so that the images do not have T2-contrast. A benefit of the sequence is that four image sets with quite different tissue contrast are obtained:

1) an in-phase image,

2) an out-of-phase image

3) a water only image and

4) a fat only image.

The out-of-phase images are sometimes useful particularly in abdominal imaging, since the border between fatty and non-fatty tissues appears dark.

This is due to destructive interference of out-of-phase fat and water signals in voxels at these tissue boundaries. The Dixon method is normally a very robust fat suppression technique.

Water excitation:

Fat suppression can also be done by exciting only the water spins and leaving the fat spins unaffected.

This is normally achieved by using a special type of RF pulse known as a binomial pulse. In fact, binomial pulses are actually a set of RF pulses

whose net effect is to produce a 90° pulse for the water spins and a 0° pulse for the fat spins. These binomial pulses are a bit longer in duration than the normal excitation pulses but since no spoiler gradient is required and there is no delay to wait for relaxation to occur, it is a rather quick way to achieve fat suppression.

The set of pulses that make up a binomial pulse are related by the binomial condition and there are many possible combinations. To illustrate how binomial pulses can be used for fat suppression, consider a binomial pulse made up of a set of three RF pulses that induce 22.5°, 45°, and 22.5° flip angles, respectively, with the time between the pulses set such that the fat spins, which are off-resonance compared to the water spins, Precess about the z-axis by 180°. In this case, the net tip angle for the on resonance water spins is the sum of the three tip angles, which is 90°. The fat spins are tipped by 22.5°by the first RF pulse but by the time the second RF pulse is applied they will have precessed to the other side of the transverse plane. Thus, the net effect of the first RF pulse plus the first delay time is equivalent to a -22.5° tip angle. The second RF pulse then tips the fat spins through 45°; from -22.5° to22.5°. Again the precession of the fat spins brings them to -22.5° and the final RF pulse, with a tip angle of 22.5°, tips the fat spins back to 0°, where they started.

Note that if the tip angles are not exactly equal to 22.5°, 45° and 22.5°, respectively, the net tip angle for the water will not be exactly equal to 90° but the tip angle for the fat spins will still be 0°, as long as the effective tip angles are in the ratio 1:2:1. Thus, fat suppression using binomial pulses is not sensitive to RF pulse spatial non uniformity (i.e. flip angle changing with position). This technique primarily relies on having the correct inter pulse delays to suppress the fat signal.

Chapter five

5. Methodology

This study was carried out using a GE super conducting magnet operating at 1.5 T.

A phantom was built specially for this study by local materials.

5.1 Materials (Of the Phantom).

In this study, fabricated phantom is used. The body of the phantom use from local materials (distilled water, vegetable oil and bottle of poly ethylene).

It used poly ethylene because it is stable, non-hazardous, cheap, easy to handle and most important it mimic the real organ characteristics. The phantom is compact and also portable that can be well suited for reassembly in multi-center research setting.

The phantom was took shape of bottle, consist of three bottles, first bottle filled with distilled water 350ml, second was filled with vegetable oil 350ml and the last was filled with distilled water 175ml and vegetable oil 175ml.

5.2 Procedure

Poly ethylene, distilled water and vegetable oil.

The phantom proves the validity of the pulse sequence used in the gradient echo systems to produce fat suppression image.

5.3 Parameters

The phantom was placed at the center of the magnet 1.5T GE, and a pulse sequence protocol was gradient echo& spin echo, was taken slice thickness (ST) 8mm the parameters were as in .

Table (1) Machine basic settings

Techniques / Parameter	TR	TE	FOV	TI
Spin echo T2	580	88.7 / EF	33 × 30	-
Spin echo T1	100	9.3 / EF	33 × 30	-
T2 Flair	8802	143 / EF	33 × 33	2200
STIR	3300	46.4 /EF	33 × 33	1400

The parameters were selected to produce the image as shown in (fig1) below, which is spin echo pulse sequence.

Total scan time for each bottle was same (5 minute).

A region of interest (ROI) was selected 0.5cm2 which was selected in circular shape for each image.

And the image intensity were measured by _RA_ application (**Product information: Product:** Radi-Anti Dicom viewer; **Version:** 2.2.5.10715 (32-bit)), the results were taken and reported in table (2).

5.4 Data Analysis

After all the scanned images were obtained, they were applied to a computer program (Radi-Anti), reading the intensity of the images. A region of interest (ROI) was chosen (circular area 0.5cm^2) for both phantom and patient to read the intensities of.

Fig(5.1) the phantom consist of three bottles

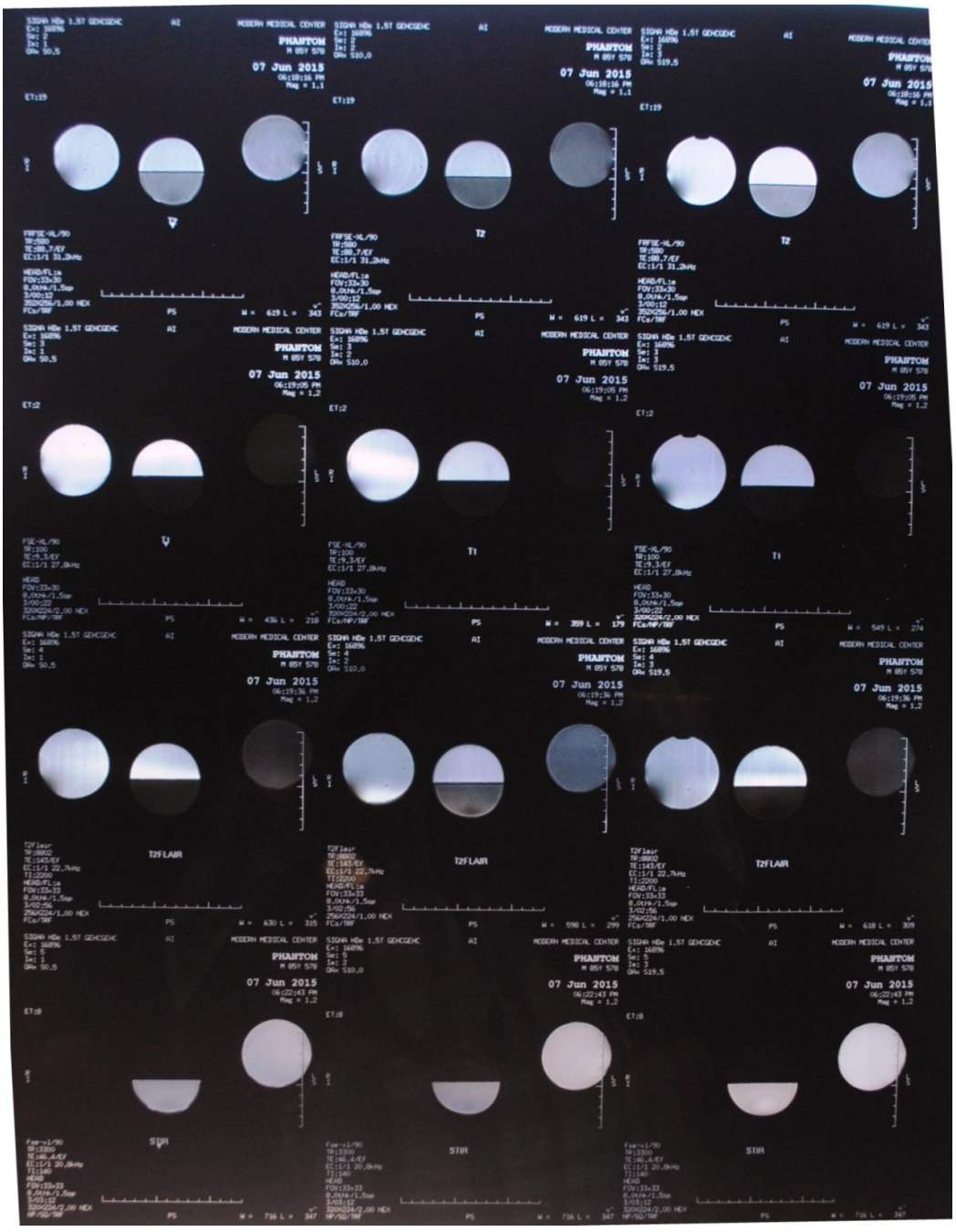

Fig(5.2) Modern Medical Center Image taken by 1.5T GE

Chapter Six

6. Results & Discussions

6.1 T2 image

Slice 1/10 area= .05cm² 46 PX

Three bottles as one phantom show the intensity on table (6.1) bellow:

	Water bottle		Mix water &oil				Oil bottle	
			Water		Oil			
	mean	±SD	mean	±SD	Mean	±SD	mean	±SD
	327.26	20.46	262.8	7.86	165.22	4.78	148.00	4.56
	268.30	14.12	275.41	18.77	163.46	3.63	156.78	3.08
	300.11	06.36	312.50	11.14	164.24	4.40	172.35	3.86
AVG	298.55	13.65	283.57	12.95	164.31	4.27	159.04	3.81

Table (6.1) intensities of the T2 image indifferent three bottles

which Was measure from image(6.1) collecting using T2 Weight Image.

The intensity value for the pure water was **298.55 , ± 13.65 SD**, while the value for water and oil from the mix consequently**was283.57, 12.95 ± SD,** And this due to interaction between the two fluid in the mixture.

There is no big different between water & oil in intensities, and this not available in medical diagnosis because need to see details.

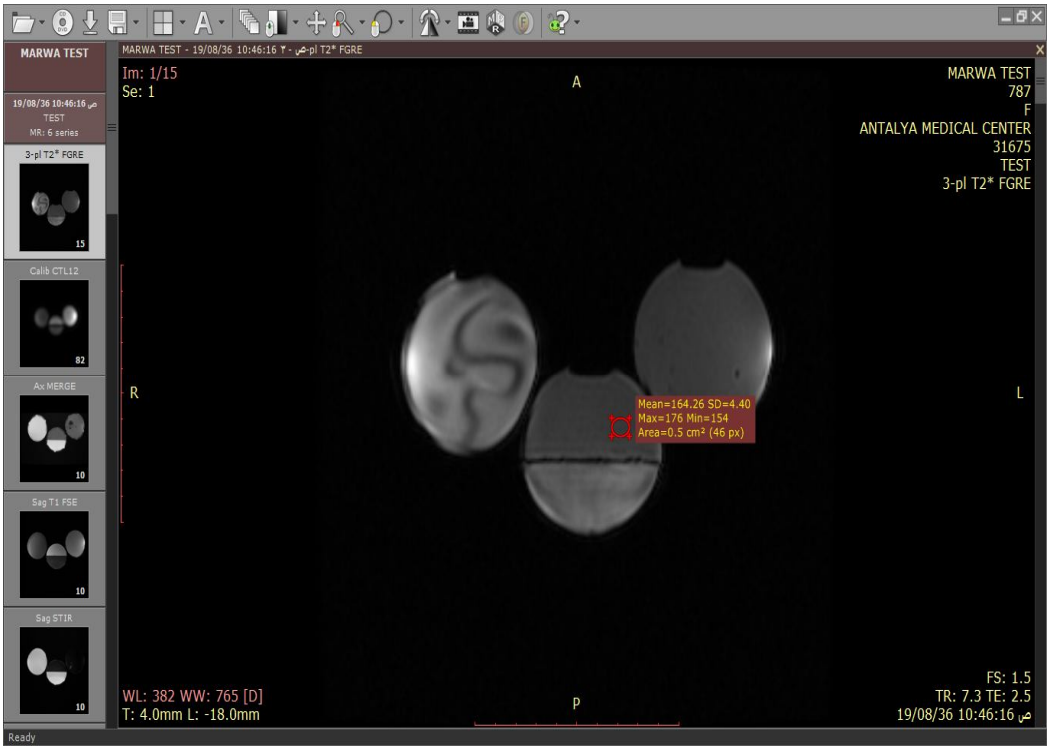

Figure (6.1) T2 image taken by GE MRI 1.5T in Antalya medical center

We Notice that there an artifact in the water image which is caused by inhomogeneity of the magnetic.

The intensity of the water from the table and images are high than those of the oil.

The difference between two intensities (of water & oil) is not large $\approx$ 140, (298.55-159.04) = 139.51$\approx$ 140.

Although this difference was sufficient to show different contrast.

The chart of fig 6.2 show T2 image technique intensity for different fluids.

The chart below show T2 image technique intensity.

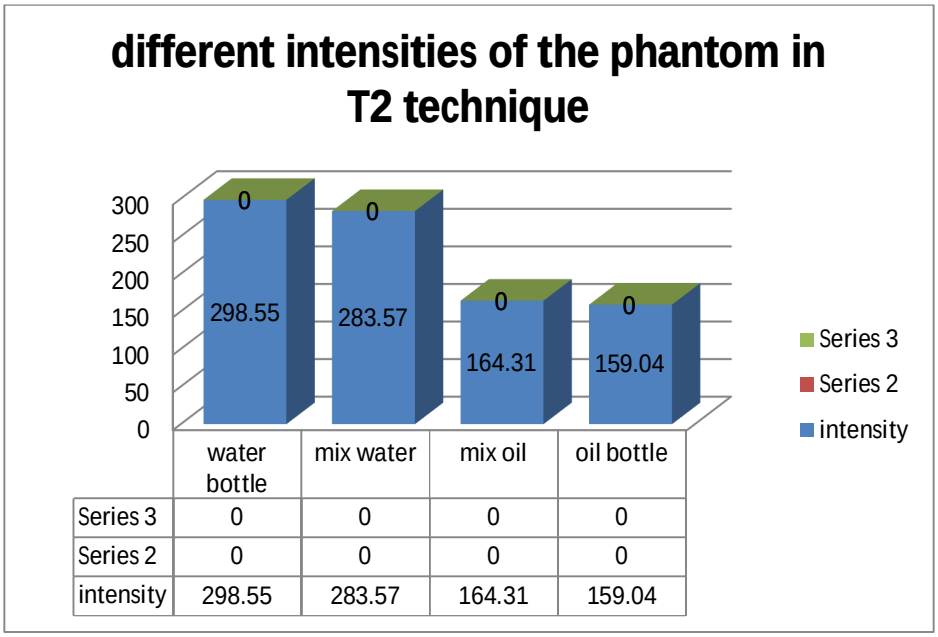

Fig (6.2) T2 image technique chart

6.2 Sag T1 image

Slice 1/10 area= .05cm² 247 PX

Three bottles as one phantom show the intensity on table (6.2) bellow:

	Water bottle		Mix water &oil				Oil bottle	
			Water		Oil			
	mean	±SD	mean	±SD	mean	±SD	mean	±SD
	676.79	32.12	395.28	20.16	832.36	16.84	821.64	18.48
	579.03	23.64	313.82	18.64	869.26	19.69	805.79	15.14
	486.96	20.35	362.50	17.87	1011.41	34.10	1098.68	33.32
AVG	579.93	25.37	357.20	18.88	904.34	23.54	908.70	22.31

Table (6.2) intensities of Sag T1 image indifferent three bottles

Intensity values in reverse order which the value from water was 579.93 ,± 25.37 SD, while value of the oil was 908.70, ±22.31 SD

Notice that water bottle has high intensity (579.93, ±25.31 SD) than mix water intensity (357.20, ±18.88 SD) that was due to artifact in the water bottle caused by inhomogeneity of the magnet,

Also different between (water & oil) intensities are narrow≈ 330 to 550, has low contrast.

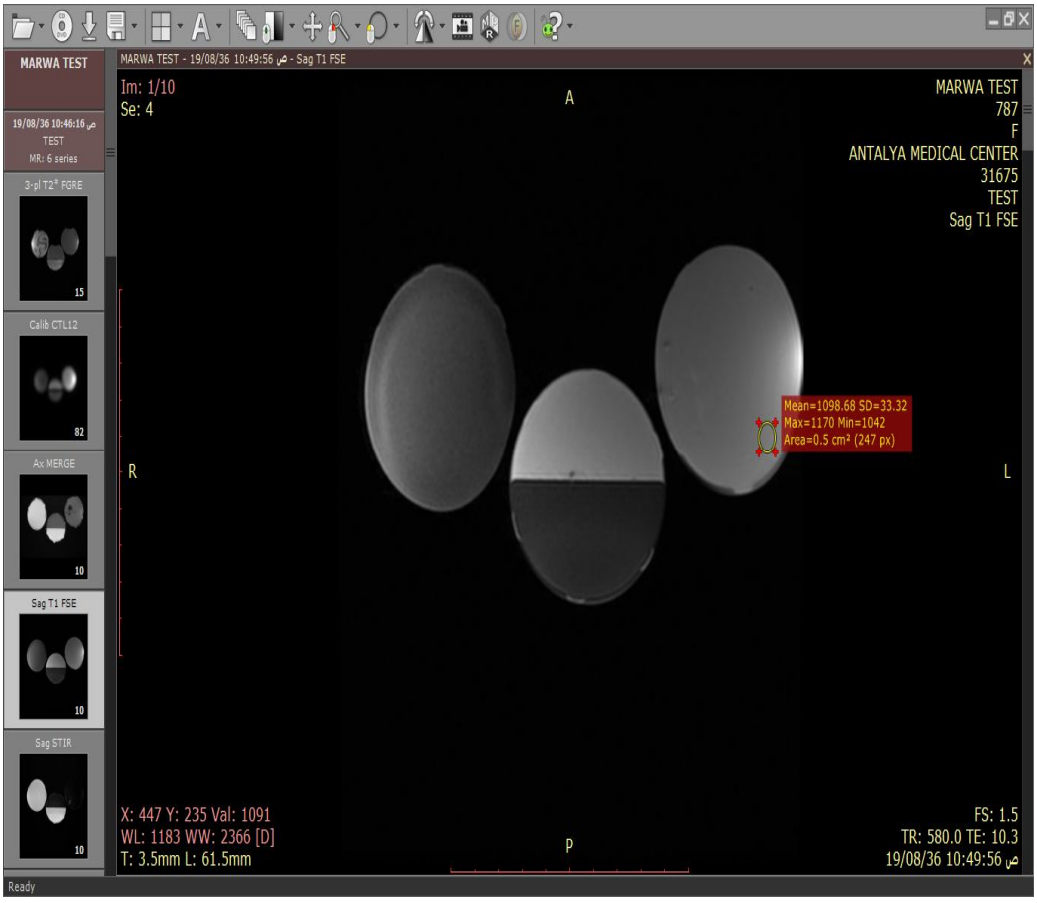

Figure (6.3) Sag T1 image taken by GE MRI 1.5T in Antalya medical center

Water in this technique seems darker than oil.

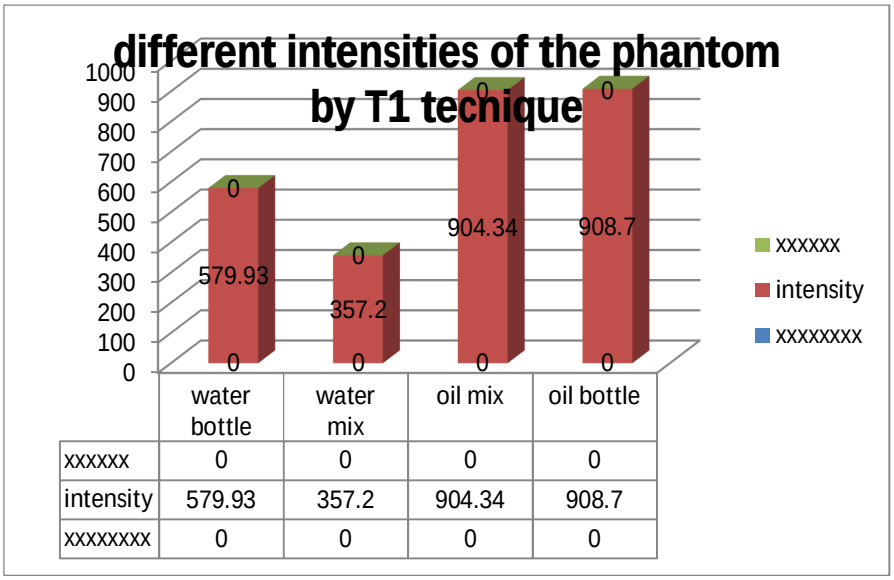

Fig (6.4) T1 image technique chart

In this chart see clearly blurring in water bottle image

6.3- Sag STIR

Area= 0.5cm, 225PX.

Three bottles as one phantom show the intensity on table (6.3) bellow:

	Water bottle		Mix water &oil				Oil bottle	
			Water		Oil			
	mean	±SD	mean	±SD	mean	±SD	mean	±SD
	1056.51	6.71	1058.36	15.83	37.03	8.75	33.17	8.25
	1047.45	7.38	1050.53	08.97	32.47	8.95	36.81	6.39
	1029.96	8.38	1092.15	17.00	61.75	7.84	53.85	14.97
AVG	1044.64	7.49	1067.01	13.94	43.75	8.51	41.28	9.87

Table (6.3) intensities of Sag STIR image indifferent three bottles

We noticed that , the value in standard deviation (SD) ≈ 14.

Notice that water bottle had high intensity (1044.64, ±7.49 SD), while water in mixture bottle had value(1067.01, ±13.94SD) different in value refer to inhomogeneity of the magnet.

The oil bottle had low intensity(41.28, ±9.87SD)), while oil in mixture bottle had value(43.75, ±8.51SD), noticed that small different between two intensities.

The range between two intensities of (water & oil) is so expand ≈ 1000.

That expand range enable to see more details, so it's Has high contrast.

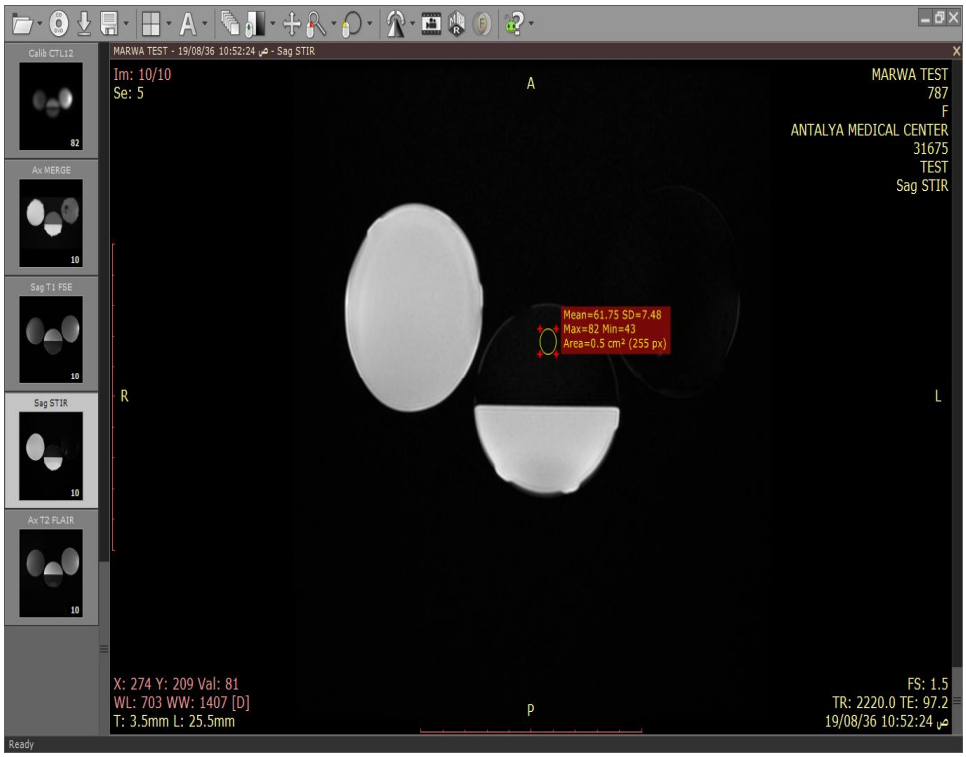

Figure (6.5) Sag STIR image taken by GE MRI 1.5T in Antalya medical center.

In this technique suppress the fat, so the oil was seemed black, because contributed nothing. Although of that, the oil has small value like (33.17) from inhomogeneity of the magnet.

The chart below show Sag STIR image technique intensity.

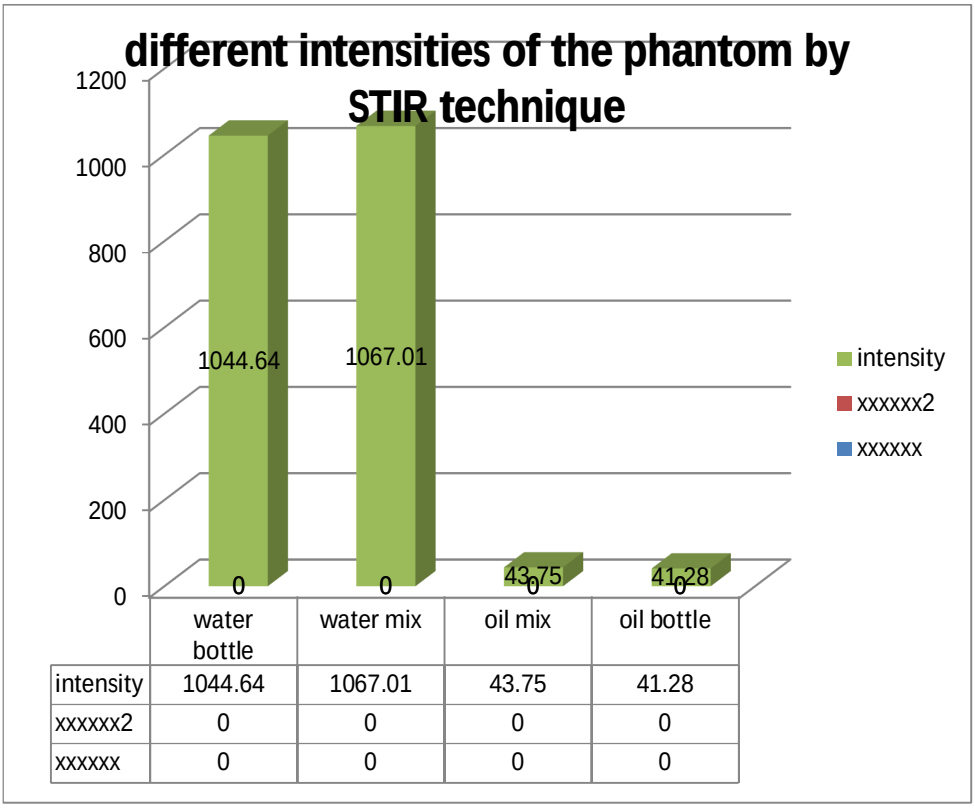

Fig (6.6)STIR image technique chart

6.4 AX T2 FLAIR image

Area= 0.5cm² 65PX

Three bottles as one phantom show the intensity on table (6.4) bellow:

	Water bottle		Mix water &oil				Oil bottle	
			Water		Oil			
	mean	±SD	mean	±SD	mean	±SD	mean	±SD
	319.46	10.06	253.37	9.71	498.32	11.29	483.68	11.38
	292.42	9.30	239.14	13.52	492.22	12.24	422.82	6.77
	353.72	7.06	236.68	16.53	478.98	12.83	399.55	7.66
AVG	321.87	8.81	243.06	13.25	489.84	12.12	435.35	8.60

Table (6.4) intensities of AX T2 FLAIR image indifferent three bottles

There is low artifact, notice that in a suitable value in standard deviation (SD) ≈ 13.

Notice that water bottle had high intensity (321.87, ±8.81 SD), while water in mixture bottle had value(243.06, ±13.25SD) different in value refer to inhomogeneity of the magnet.

The oil bottle had low intensity(435.35, ±8.6SD)), while oil in mixture bottle had value(489.84, ±12.12SD),

The range between two intensities of (water & oil) was so narrow ≈ 113 to 247. Has low contrast.

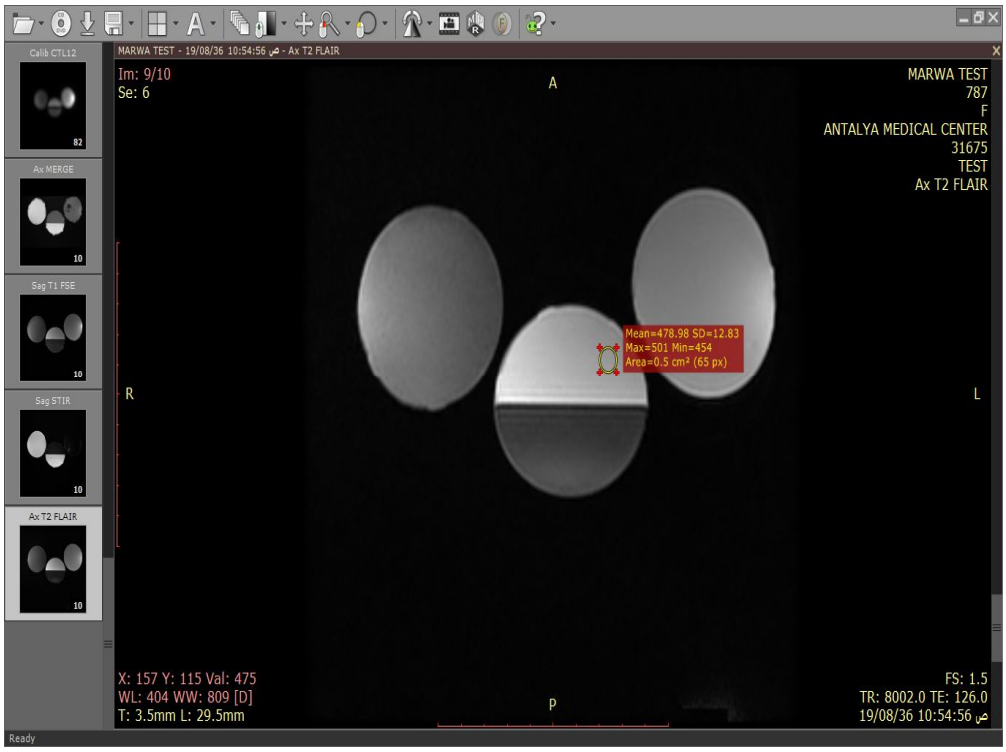

Figure (6.7) AX T2 FLAIR image taken by GE MRI 1.5T in Antalya medical center.

saw manifestly that technique.

The chart below show AX T2 FLAIR image technique intensity.

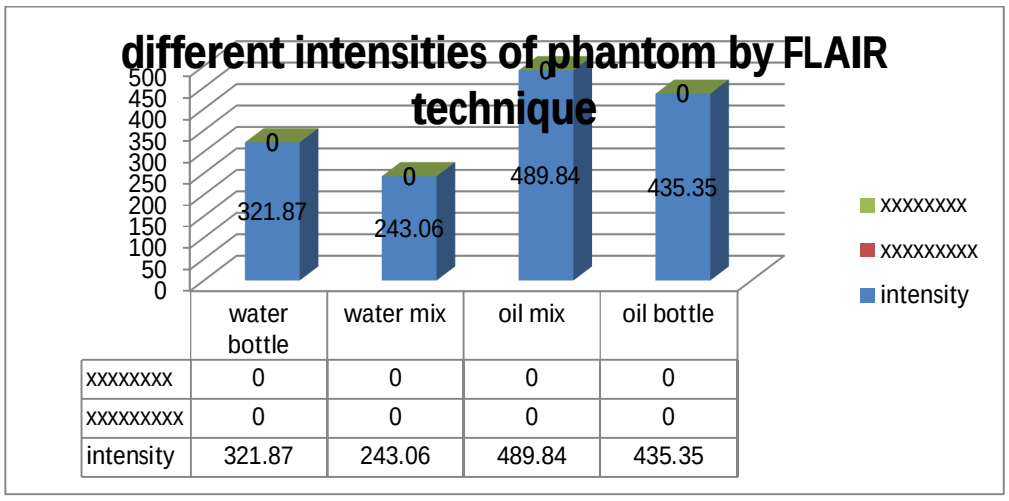

	water bottle	water mix	oil mix	oil bottle
xxxxxxxx	0	0	0	0
xxxxxxxxx	0	0	0	0
intensity	321.87	243.06	489.84	435.35

Fig (6.8)AX T2 FLAIR image technique chart

6.5 Conversation between techniques

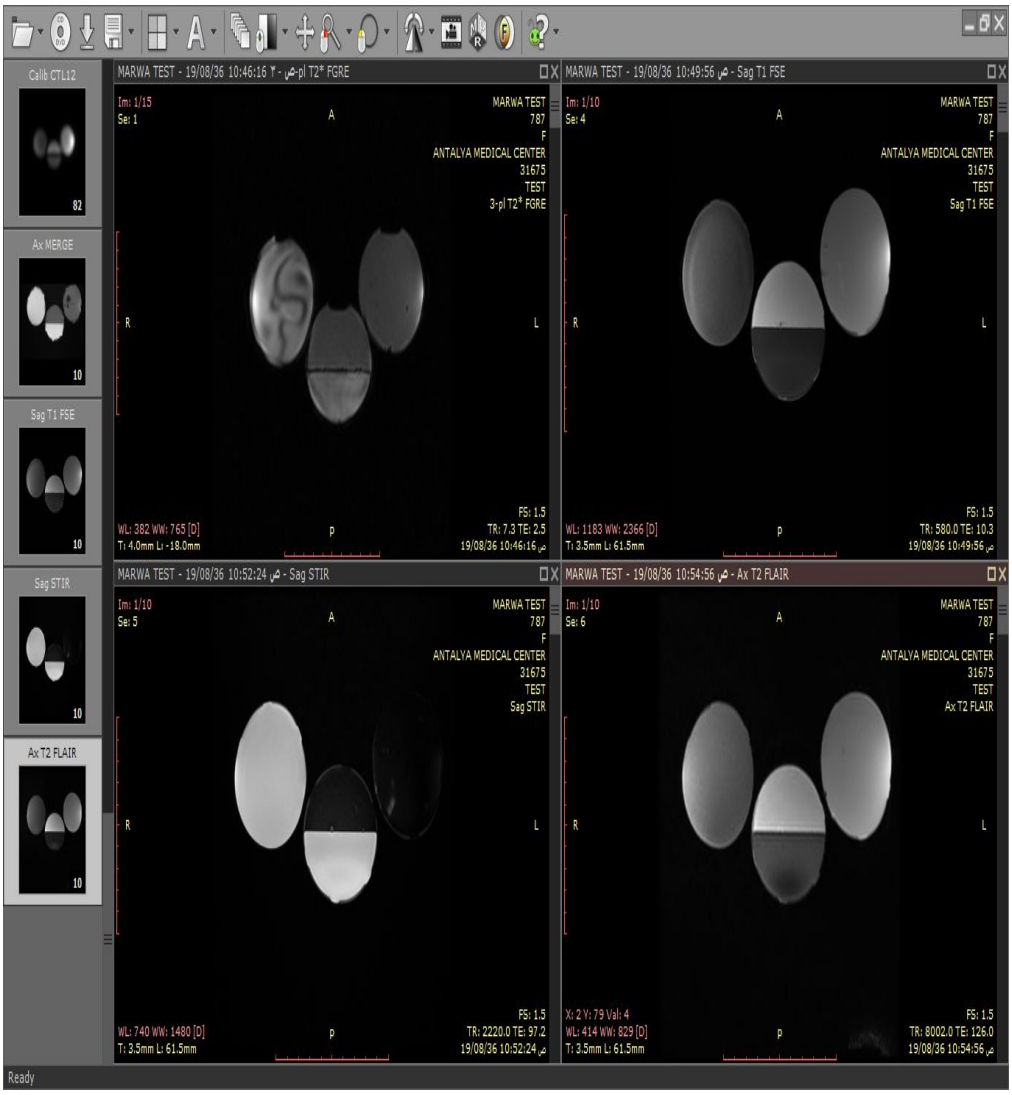

Figure (6.9) image techniques (T1, T2, STIR, FLAIR) taken by GE MRI 1.5T in Antalya medical center.

Conversation between techniques that performance.

Phantom / Techniques	Water bottle	Mix water	Mix oil	Oil bottle
AX T2	298.55	283.57	164.31	159.04
Sag T1	579.93	357.2	904.34	908.70
STIR	1044.64	1067.01	43.75	41.28
FLAIR	321..87	243.06	489.84	435.35

Table (6.5) intensities of all techniques of images in different three bottles

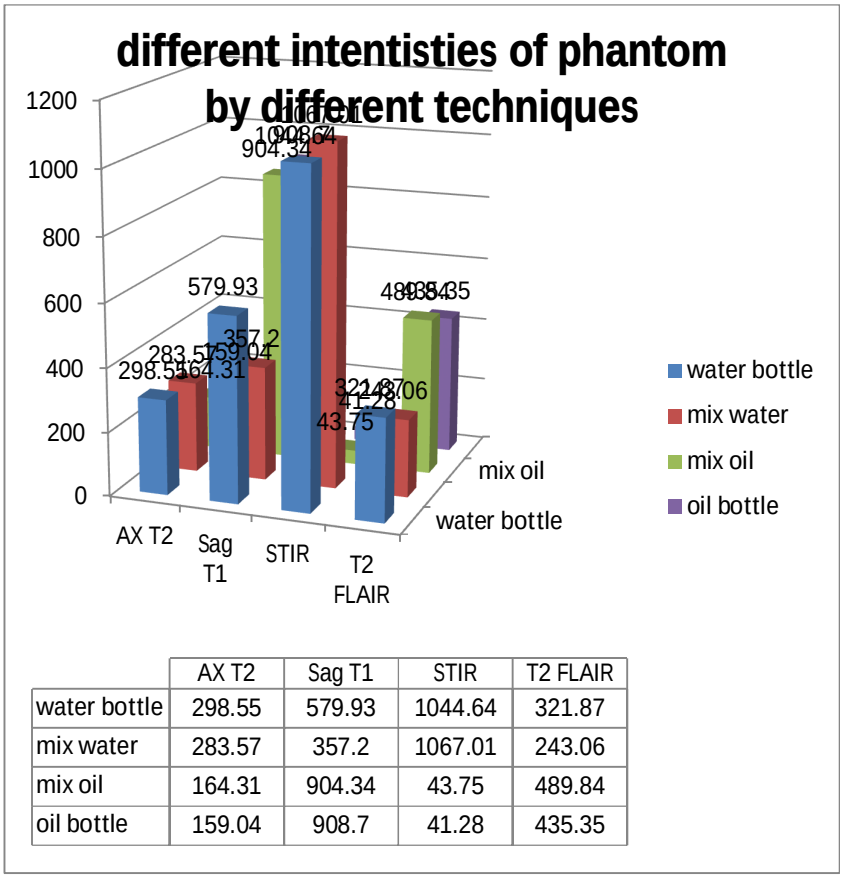

	AX T2	Sag T1	STIR	T2 FLAIR
water bottle	298.55	579.93	1044.64	321.87
mix water	283.57	357.2	1067.01	243.06
mix oil	164.31	904.34	43.75	489.84
oil bottle	159.04	908.7	41.28	435.35

Fig (6.10)Different technique chart

As regards: The system was then used to:

1. image a patient (male, aged 55) suffering of memory Missing, The patient was placed in the center of the magnet, and the head was inserted into.

Pulse was used to produce the image with parameters;

The sequences were:

Sag T1, Ax T1, Ax T2, Coronal T2, Ax T2 Flair, DWI (diffusion weighted image)

Level

Basal ganglia to skull cub

Diagnosis

- Senile brave atrophy
- Periventricular deep white Walter ischemic changes.
- The compression results between (AX T1 &Ax T2 Flair) Techniques were taken and reported in table (6,6).
  Slice=15/22 area=0.5cm² PX=50

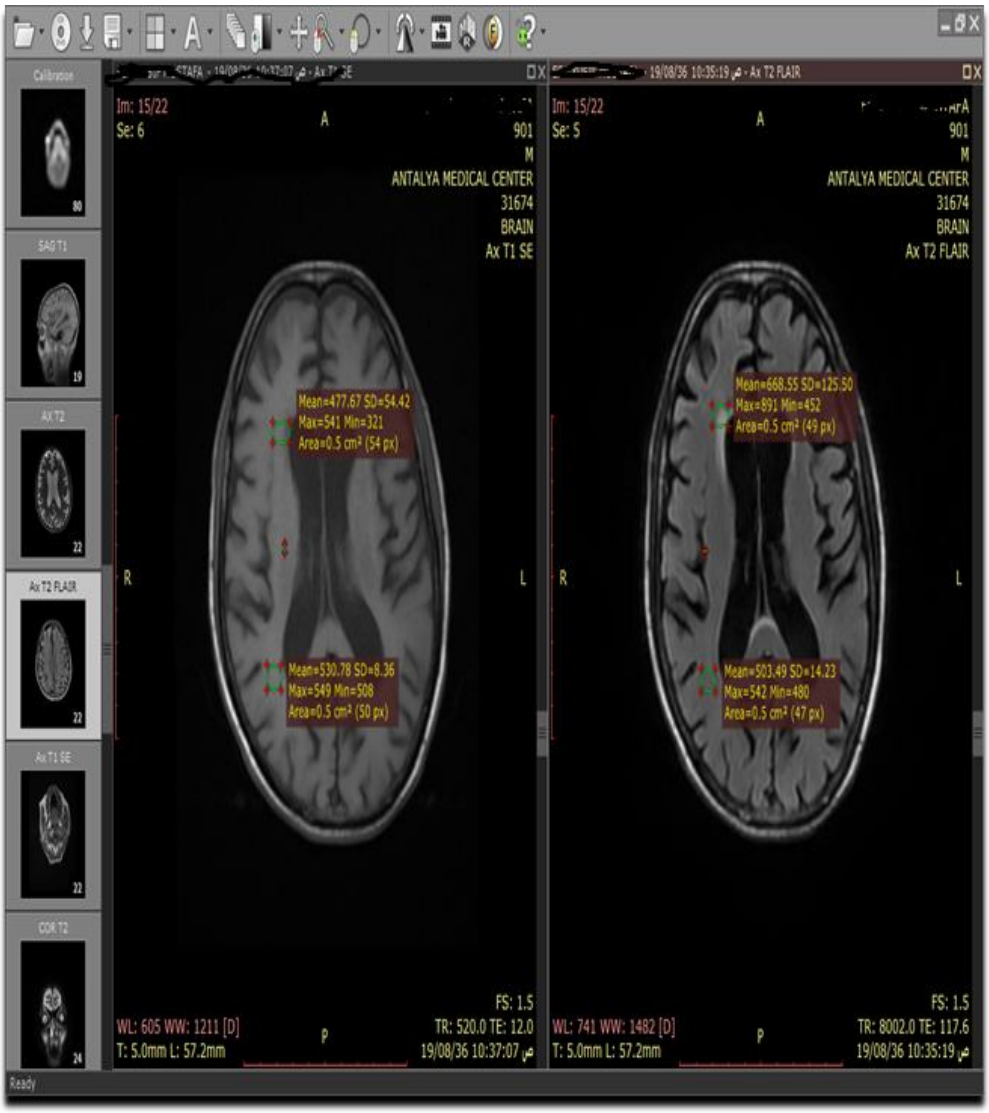

fig(6,11) comparison betweenAXT1 &AXT2 FLAIR in patient1 image used by GE MRI 1.5T Antalya medical center

AXT2 FLAIR				**AXT1**				**Patient1**
Up nor-tissue		Normal tissue		Up nor-tissue		Normal tissue		
mean	±SD	mean	±SD	mean	±SD	mean	±SD	**parameter**
668.55	**125**	**503.5**	**14**	**477.6**	**54**	**530.8**	**8.36**	**intensity**

Table(6,6)Intensities of normal & up normal tissues in AXT1 & AXT2 FLAIR Techniques in patient1 image taken by GE MRI 1.5T in Antalya medical center**.**

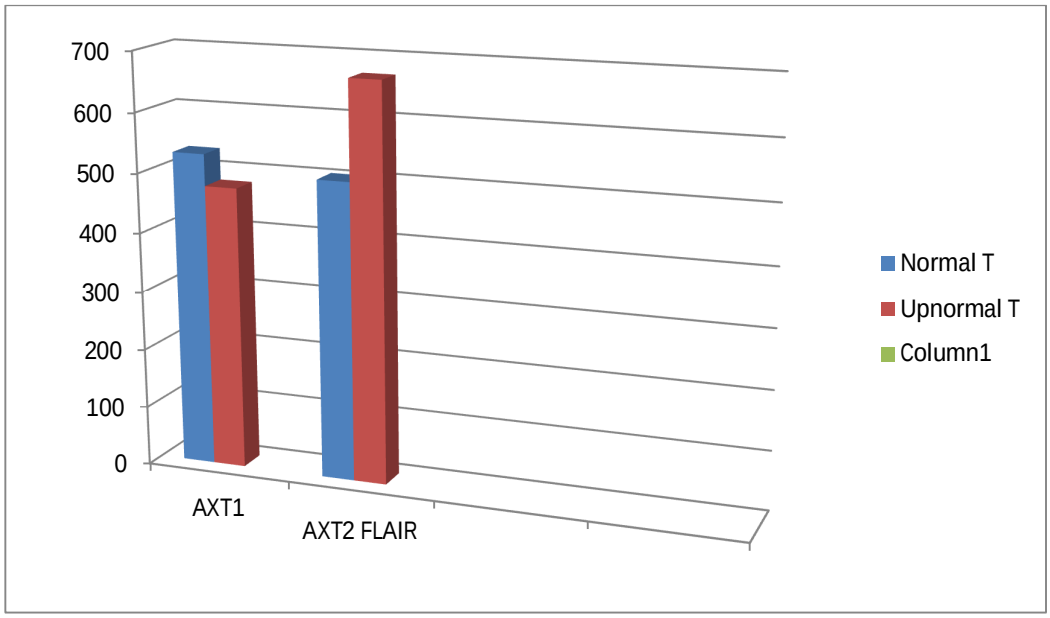

fig(6,12) Patient1 intensity chart

As in fig (6, 12) noticed that AXT2 FLAIR technique was more contrast & more detail than AXT1 technique

2. image a patient (male, aged 35) suffering of headache, The patient was placed in the center of the magnet, and the head was inserted into.

The sequences were:

Sag T1, Ax T1, Ax T2, Coronal T2, Ax T2 Flair, DWI (diffusion (weighted image

Level

Basal ganglia to skull cub

Diagnosis

Mass tumor surrounding fluid, Atrophy.

- Techniques were taken and reported in table (6,7).
- Techniques used were **AXT2 FLAIR & AXT1** as shown in fig(6, 13).

Slice=11/22 area=0.5cm² PX=70

AXT2 FLAIR				**AXT1**				**Patient2**
Up nor-tissue		Normal tissue		Up nor-tissue		Normal tissue		
mean	±SD	mean	±SD	mean	±SD	Mean	±SD	**parameter**
47	**10**	**457**	**24**	**400**	**15**	**716**	**16**	**Intensity**

Table(6,7)Intensities of normal & up normal tissues in AXT1 & AXT2 FLAIR Techniques in patient2 image taken by GE MRI 1.5T in modern medical center**.**

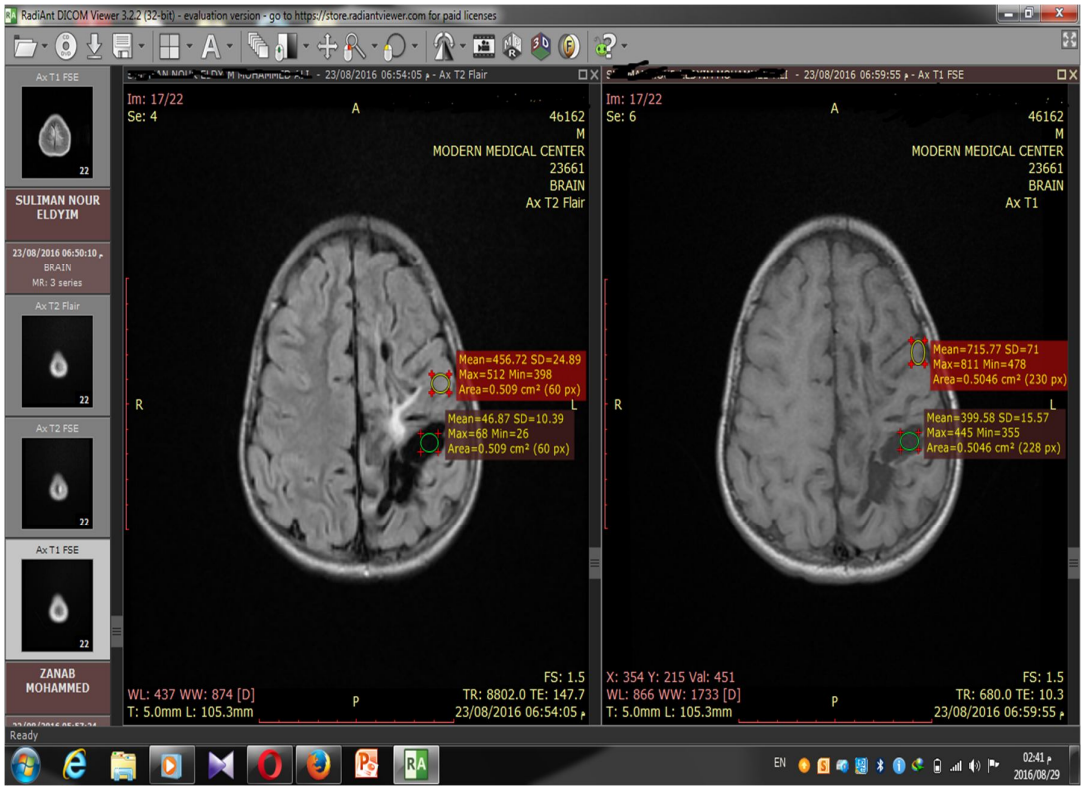

fig(6,13) comparison betweenAXT1 &AXT2 FLAIR in patient2 image

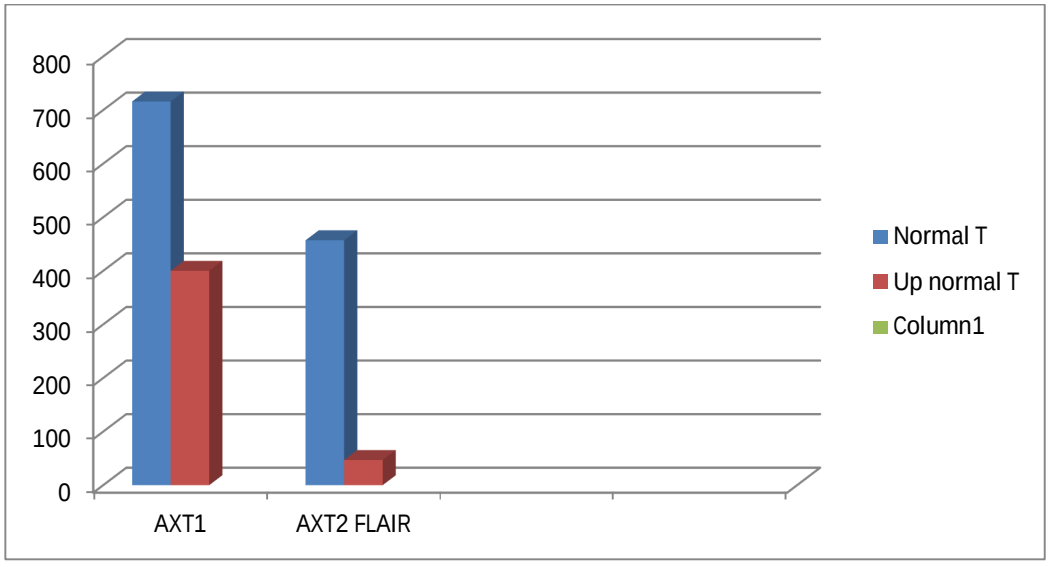

fig(6,14) Patient2 intensity chart

As in fig (6, 14) noticed that AXT2 FLAIR technique was more contrast & more detail than AXT1 technique.

3. image a patient (male, aged 35) suffering of headache, The patient was placed in the center of the magnet, and the head was inserted into.

The sequences were:

Sag T1, Ax T1, Ax T2, Coronal T2, Ax T2 Flair.

Level

Basal ganglia to skull cub

Diagnosis

Mass tumor surrounding fluid, Atrophy.

- Techniques were taken and reported in table (6,8).
- Techniques used were **AXT2 FLAIR & AXT1** as shown in fig(6, 15).

Slice= area=0.5cm² PX=

AXT2 FLAIR				**AXT1**				**Patient3**
Up nor-tissue		Normal tissue		Up nor-tissue		Normal tissue		
mean	±SD	mean	±SD	Mean	±SD	mean	±SD	**parameter**
106	**31**	**443**	**20**	**391**	**36**	**797**	**25**	**Intensity**

Table(6,7)Intensities of normal & up normal tissues in AXT1 & AXT2 FLAIR Techniques in patient3 image taken by GE MRI 1.5T in modern medical center

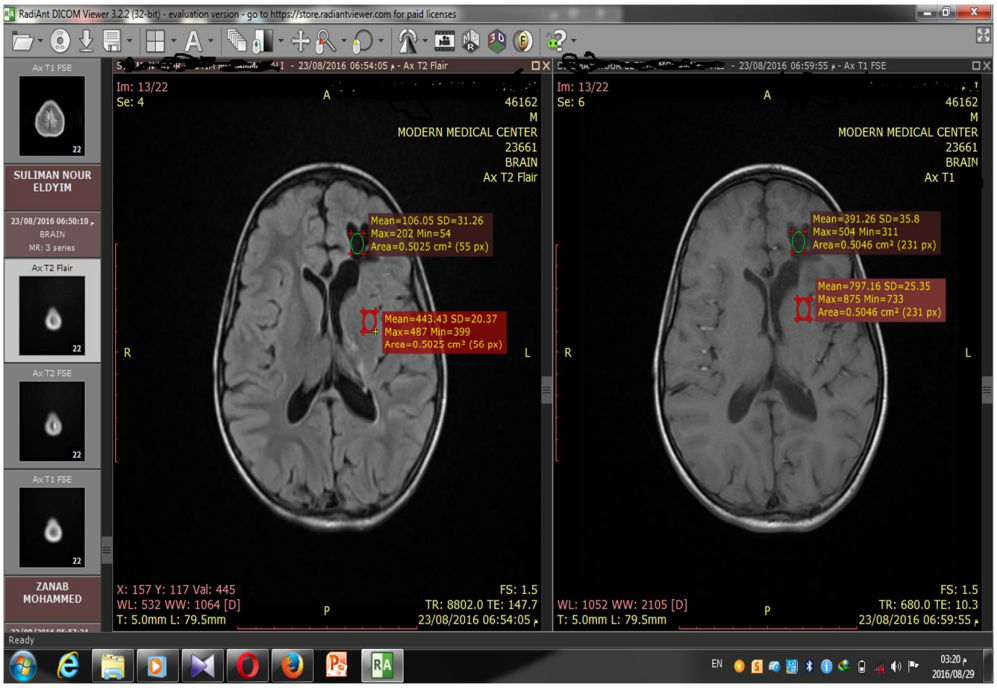

fig(6,15) comparison betweenAXT1 &AXT2 FLAIR in patient3 image taken by GE MRI1.5T in modern medical center.

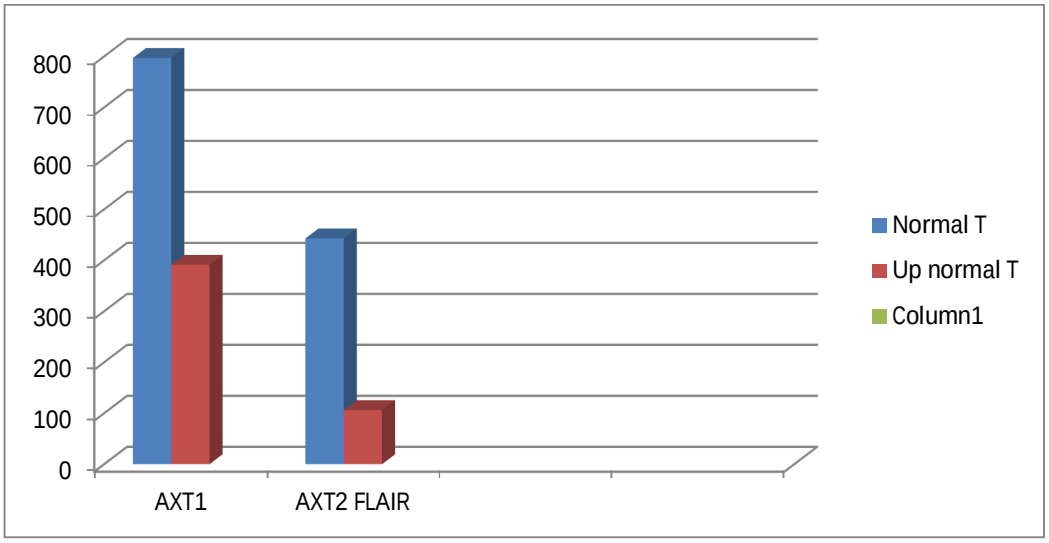

fig(6,16) Patient3 intensity chart

As in fig (6, 16) noticed that AXT2 FLAIR technique was more contrast & more detail than AXT1 technique.

4. image a patient (male, aged 65) suffering of head roll and Fainted, The patient was placed in the center of the magnet, and the head was inserted into.

The sequences were:

Sag T1, Ax T1, Ax T2, Coronal T2, Ax T2 Flair.

Level

Basal ganglia to skull cub

Diagnosis

Infraction, clot blood cell, Atrophy.

- Techniques were taken and reported in table (6,9).
- Techniques used were **AXT2 FLAIR & AXT1** as shown in fig(6, 17).

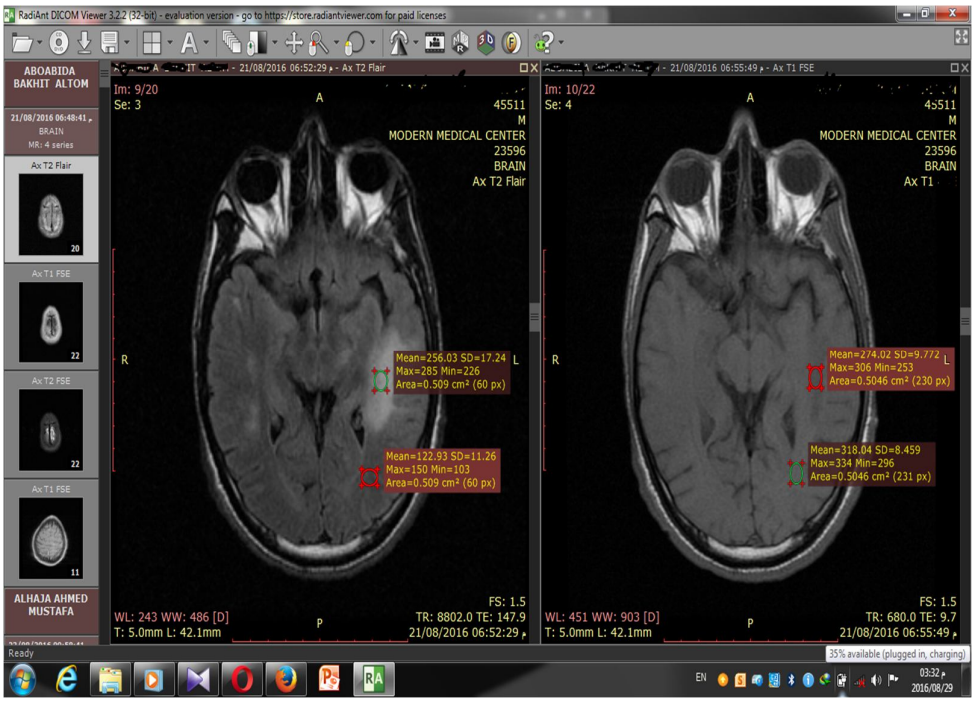

fig(6,17) comparison betweenAXT1 &AXT2 FLAIR in patient4 image taken by GE MRI1.5T in modern medical center.

Slice= 9/20, 12/22. Area=0.5cm². PX=200

AXT2 FLAIR				**AXT1**				**Patient4**
Up nor-tissue		Normal tissue		Up nor-tissue		Normal tissue		
mean	±SD	mean	±SD	mean	±SD	mean	±SD	**parameter**
256	**17**	**123**	**11**	**274**	**10**	**318**	**8**	**Intensity**

Table(6,8)Intensities of normal & up normal tissues in AXT1 & AXT2 FLAIR Techniques in patient4 image taken by GE MRI

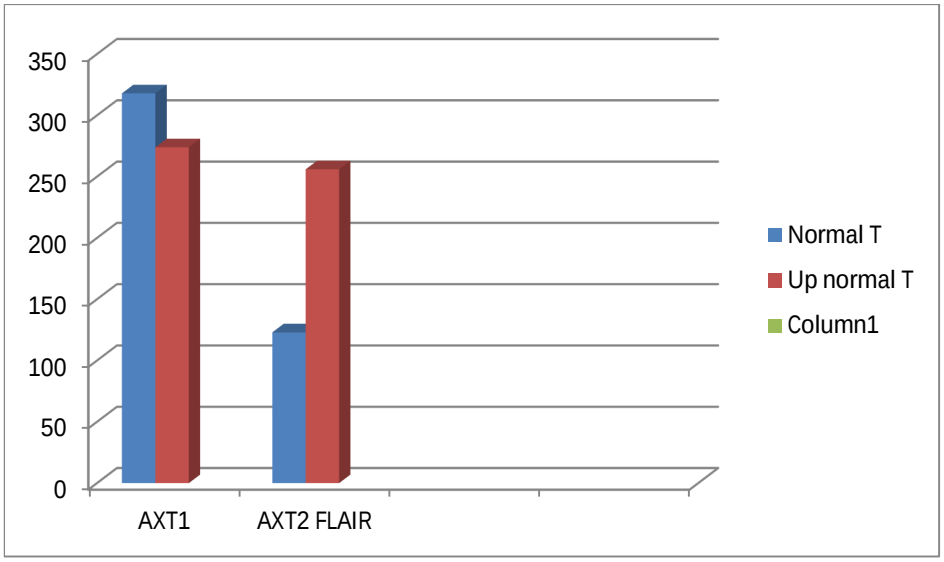

fig(6,18) Patient4 intensity chart**.**

As in fig (6, 18) noticed that AXT2 FLAIR technique was more contrast & more detail than AXT1 technique

5. image a patient (female, aged 13) suffering of missing memory, The patient was placed in the center of the magnet, and the head was inserted into.

The sequences were:

Sag T1, Ax T1, Ax T2, Coronal T2, Ax T2 Flair.

Level

Basal ganglia to skull cub

Diagnosis

Beginning of Atrophy and multiples sclerosis.

- Techniques were taken and reported in table (6, 10).
- Techniques used were **AXT2 FLAIR & AXT1** as shown in fig(6, 19).

Slice=11/22. Area=0.5cm² PX=230.

AXT2 FLAIR				**AXT1**				**Patient5**
Up nor-tissue		Normal tissue		Up nor-tissue		Normal tissue		
mean	±SD	mean	±SD	mean	±SD	mean	±SD	**parameter**
186	**38**	**143**	**15**	**471**	**14**	**471**	**19**	**Intensity**

Table(6,9)Intensities of normal & up normal tissues in AXT1 & AXT2 FLAIR Techniques in patient5 image taken by GE MRI 1.5T in modern medical center

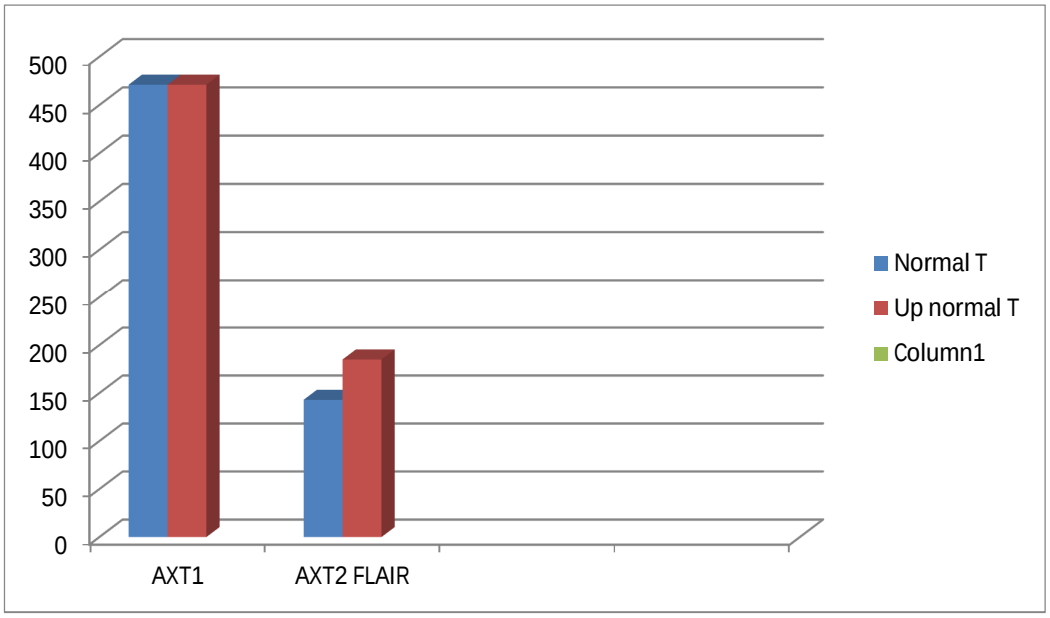

fig(6,19) Patient5 intensity chart.

As in fig (6, 19) noticed that AXT2 FLAIR technique was more contrast & more detail than AXT1 technique

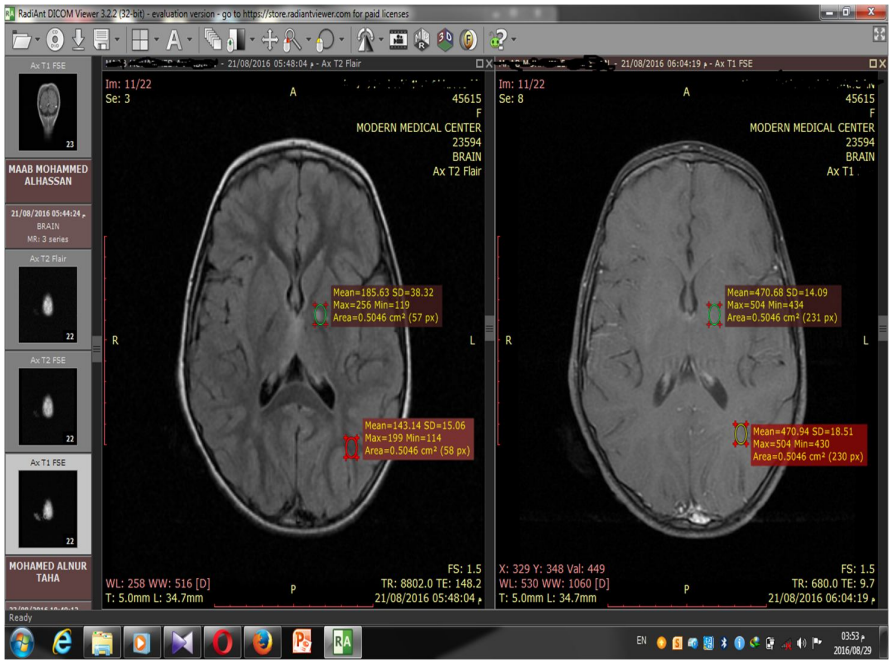

fig(6,20) comparison betweenAXT1 &AXT2 FLAIR in patient5 image taken by GE MRI1.5T in modern medical center.

6. image a patient (male, aged 42) suffering of headache, The patient was placed in the center of the magnet, and the head was inserted into.

The sequences were:

Sag T1, Ax T1, Ax T2, Coronal T2, Ax T2 Flair.

Level

Basal ganglia to skull cub

Diagnosis

Clot blood cell**.**

- Techniques were taken and reported in table (6,11).
- Techniques used were **AXT2 FLAIR & AXT1** as shown in fig(6, 21).

Slice= 18/22. area=0.5cm² PX=60.

AXT2 FLAIR				**AXT1**				**Patient6**
Up nor-tissue		Normal tissue		Up nor-tissue		Normal tissue		
Mean	±SD	mean	±SD	mean	±SD	mean	±SD	**parameter**
73	**15**	**28**	**8**	**168**	**10**	**207**	**24**	**Intensity**

Table(6,10)Intensities of normal & up normal tissues in AXT1 & AXT2 FLAIR Techniques in patient6 image taken by GE MRI

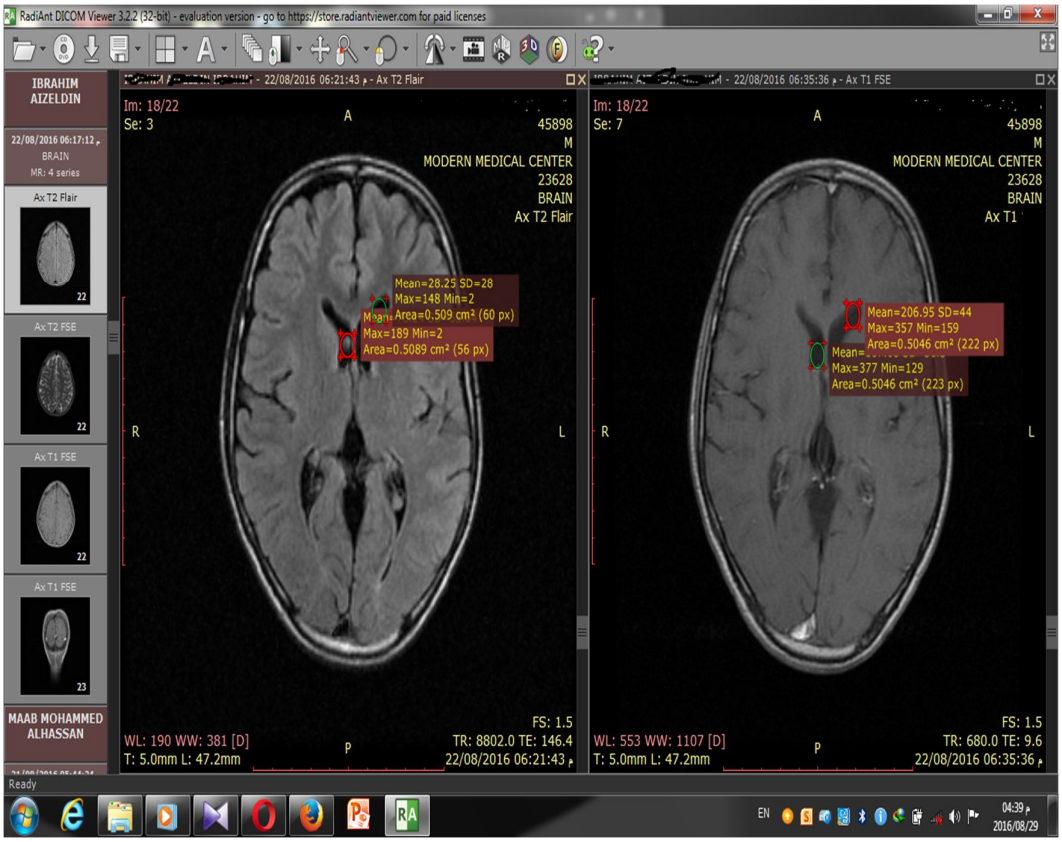

fig(6,21) comparison betweenAXT1 &AXT2 FLAIR in patient6 image taken by GE MRI1.5T in modern medical center.

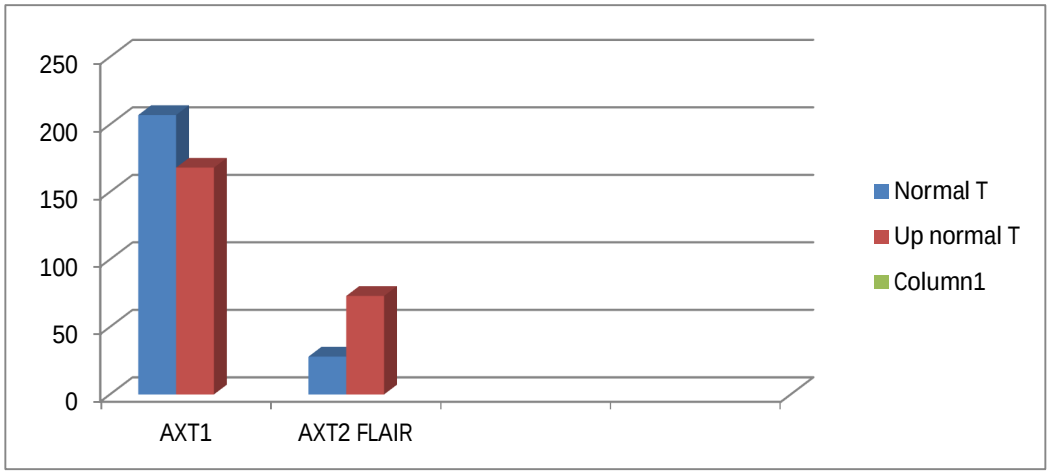

fig(6,22) Patient6 intensity chart

As in fig (6, 22) noticed that AXT2 FLAIR technique was more contrast & more detail than AXT1 technique.

7. image a patient (male, aged 57) suffering of headache, head roll The patient was placed in the center of the magnet, and the head was inserted into.

The sequences were:

Sag T1, Ax T1, Ax T2, Coronal T2, Ax T2 Flair.

Level

Basal ganglia to skull cub

Diagnosis

Mass tumor surrounding fluid, Atrophy Stroke Edema.

- Techniques were taken and reported in table (6,12).
- Techniques used were **AXT2 FLAIR & AXT1** as shown in fig(6, 23).

Slice=19/22. Area=0.5cm² PX=56,230.

AXT2 FLAIR				**AXT1**				**Patient7**
Up nor-tissue		Normal tissue		Up nor-tissue		Normal tissue		
Mean	±SD	mean	±SD	mean	±SD	mean	±SD	**parameter**
309	**8**	**148**	**12**	**266**	**18**	**333**	**13**	**Intensity**

Table(6,11)Intensities of normal & up normal tissues in AXT1 & AXT2 FLAIR Techniques in patient7 image taken by GE MRI 1.5T in modern medical center.

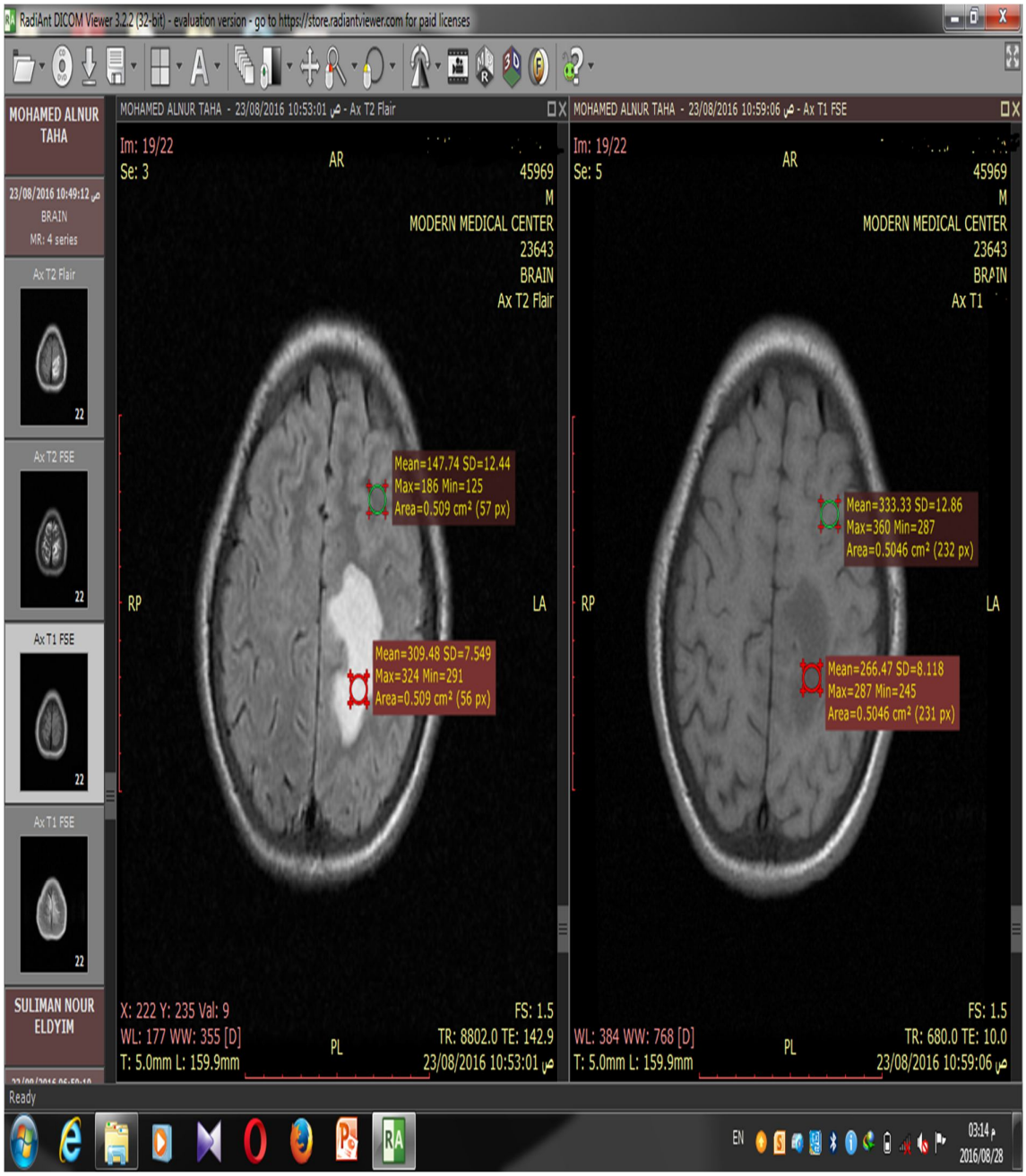

fig(6,23) comparison betweenAXT1 &AXT2 FLAIR in patient7 image taken by GE MRI1.5T in modern medical center.

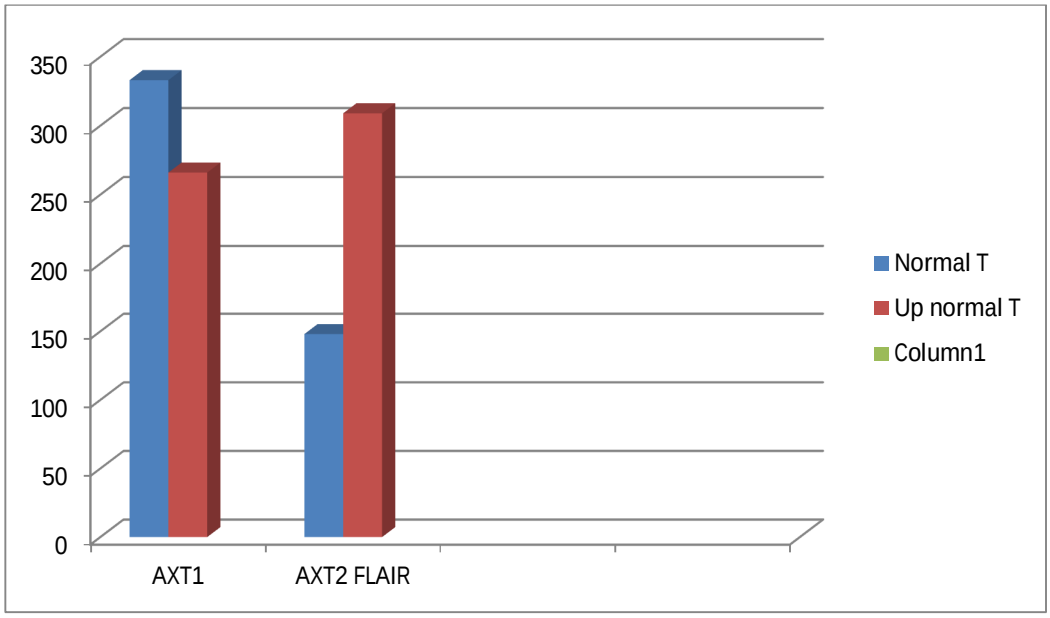

fig(6,24) Patient7 intensity chart.

As in fig (6, 24) noticed that AXT2 FLAIR technique was more contrast & more detail than AXT1 technique

8. image a patient (male, aged 35) suffering of, lack of vision headache, The patient was placed in the center of the magnet, and the head was inserted into.

The sequences were:

Sag T1, Ax T1, Ax T2, Coronal T2, Ax T2 Flair.

Level

Basal ganglia to skull cub

Diagnosis

Mass tumor surrounding fluid, Atrophy.

- Techniques were taken and reported in table (6,12).
- Techniques used were **AXT2 FLAIR & AXT1** as shown in fig(6, 25).

Slice=14/22. area=0.5cm². PX=60,230

AXT2 FLAIR				**AXT1**				
Up nor-tissue		Normal tissue		Up nor-tissue		Normal tissue		**Patient8**
mean	±SD	mean	±SD	mean	±SD	mean	±SD	**parameter**
336	**8**	**153**	**8**	**272**	**10**	**330**	**10**	**Intensity**

Table(6,12)Intensities of normal & up normal tissues in AXT1 & AXT2 FLAIR Techniques in patient8 image taken by GE MRI 1.5T in modern medical center.

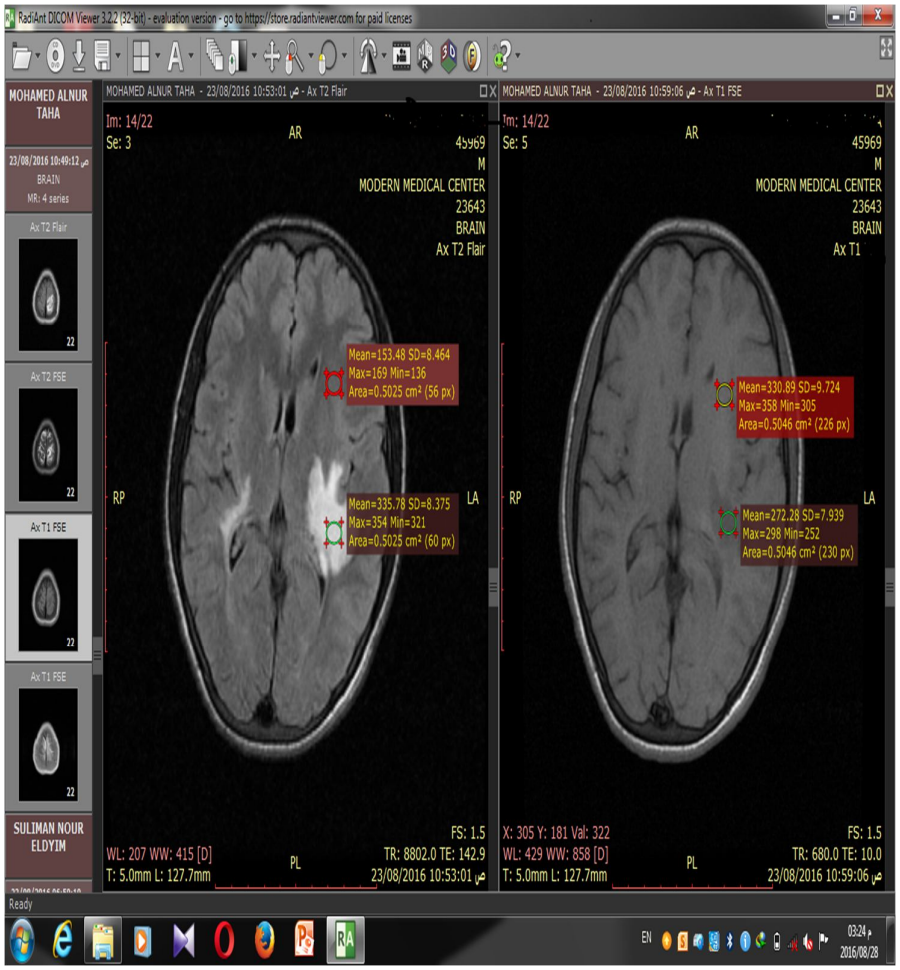

fig(6,25) comparison betweenAXT1 &AXT2 FLAIR in patient8 image taken by GE MRI1.5T in modern medical center.

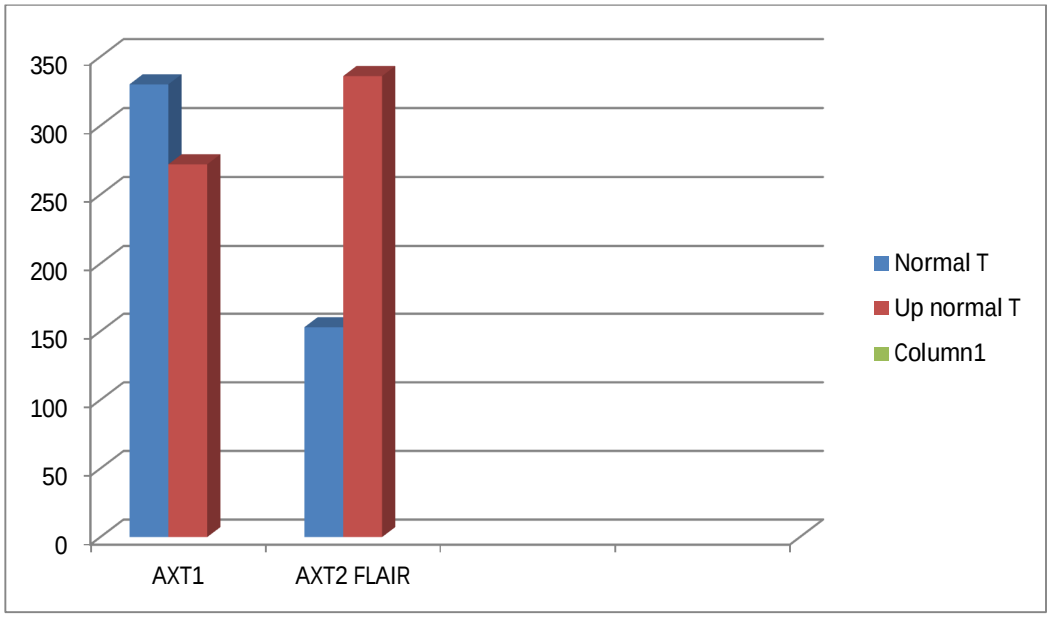

fig(6,26) Patient8 intensity chart.

As in fig (6, 26) noticed that AXT2 FLAIR technique was more contrast & more detail than AXT1 technique.

9. image a patient (female, aged 35) suffering of pain in neck, The patient was placed in the center of the magnet, and was inserted into.

The sequences were:

Coronal STIR, Ax T1, Ax T2, Coronal T2.

Diagnosis

Mass tumor surrounding fluid.

- Techniques were taken and reported in table (6,13).
- Techniques used were **COR STIR& COR T2**as shown in fig(6, 27).

Slice=9/20,11/20. Area=0.5cm². PX=330.

COR STIR				**COR T2**				
Up nor-tissue		Normal tissue		Up nor-tissue		Normal tissue		**Patient9**
mean	±SD	mean	±SD	mean	±SD	mean	±SD	**parameter**
153	**10**	**557**	**12**	**557**	**15**	**798**	**14**	**Intensity**

Table(6,13)Intensities of normal & up normal tissues in COR STIR & COR T2 Techniques in patient9 image taken by GE MRI 1.5T in modern medical center.

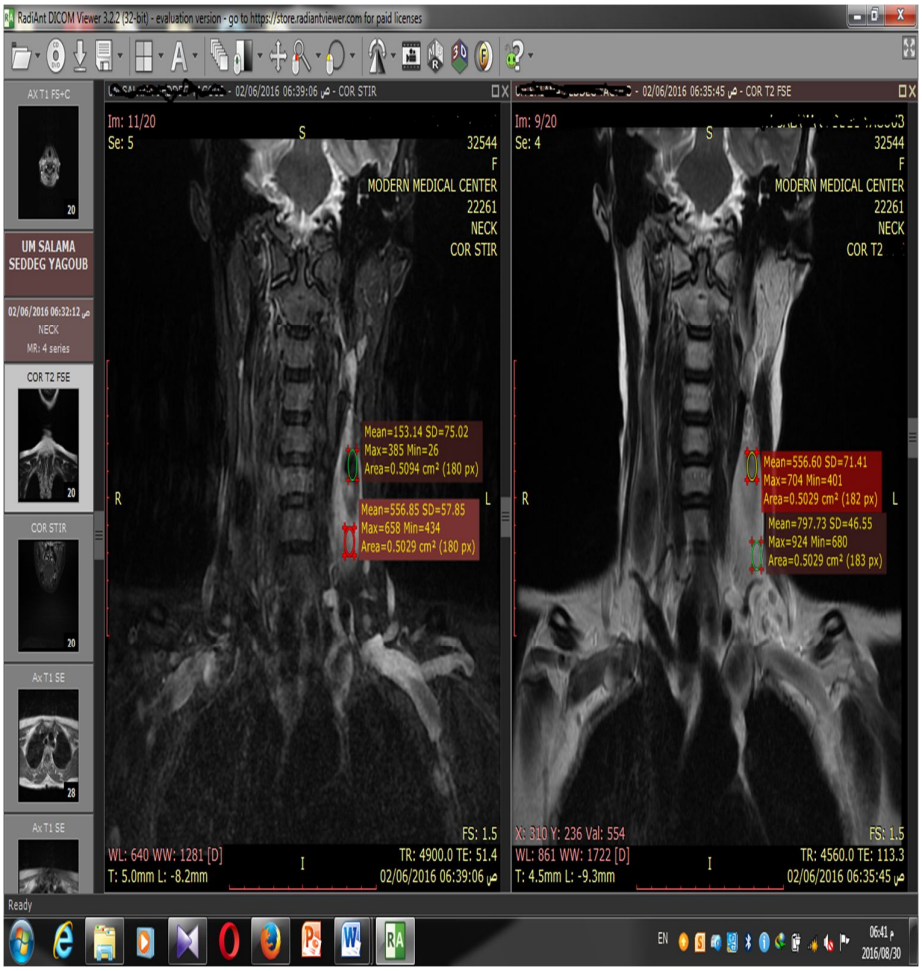

fig(6,27) comparison between COR T2 & COR STIR in patient9 image taken by GE MRI1.5T in modern medical center.

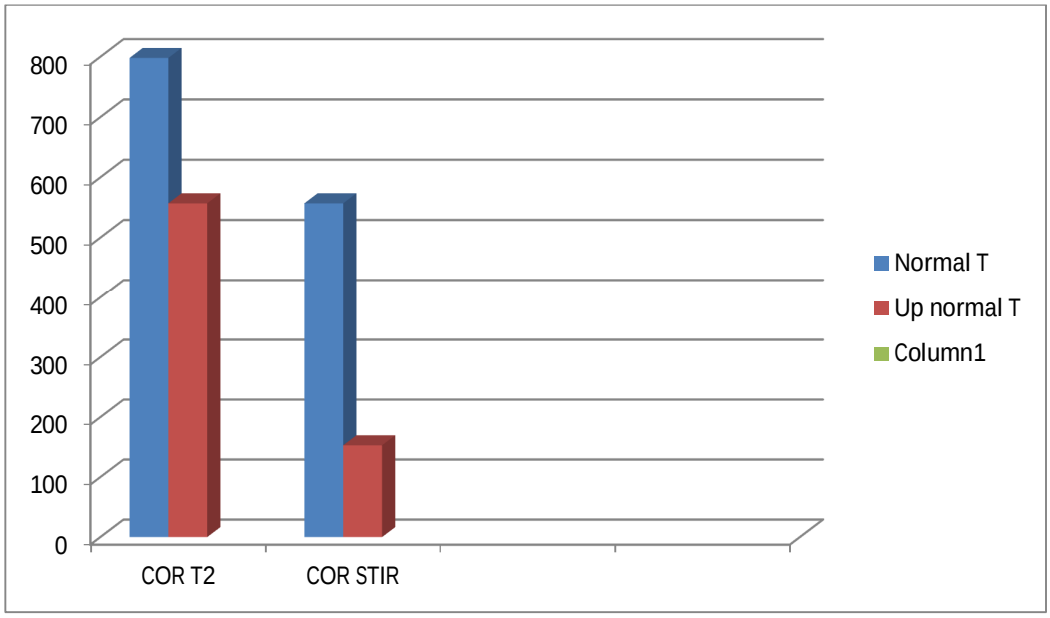

fig(6,28) Patient9 intensity chart**.**

As in fig (6, 28) noticed that COR STIR technique was more contrast & more detail than COR T2 technique.

10. image a patient (female, aged 55) suffering of pain in neck, The patient was placed in the center of the magnet, and was inserted into.

The sequences were:

AX STIR, Ax T1, Ax T2, Coronal T2.

Diagnosis

She was normal case.

- Techniques were taken and reported in table (6,14).
- Techniques used were **AX STIR & AX T2**as shown in fig(6, 29).

Slice=9/20. area=0.5cm². PX=110.

AX STIR				**AX T2**				
Up nor-tissue		Normal tissue		Up nor-tissue		Normal tissue		**Patient10**
mean	±SD	mean	±SD	mean	±SD	mean	±SD	**parameter**
221	**10**	**221**	**12**	**241**	**11**	**272**	**12**	**Intensity**

Table(6,14)Intensities of normal & up normal tissues in AX STIR & AXT2 Techniques in patient10 image taken by GE MRI 1.5T in modern medical center.

fig(6,29) comparison between AX T2 &AX STIR in patient9 image taken by GE MRI1.5T in modern medical center.

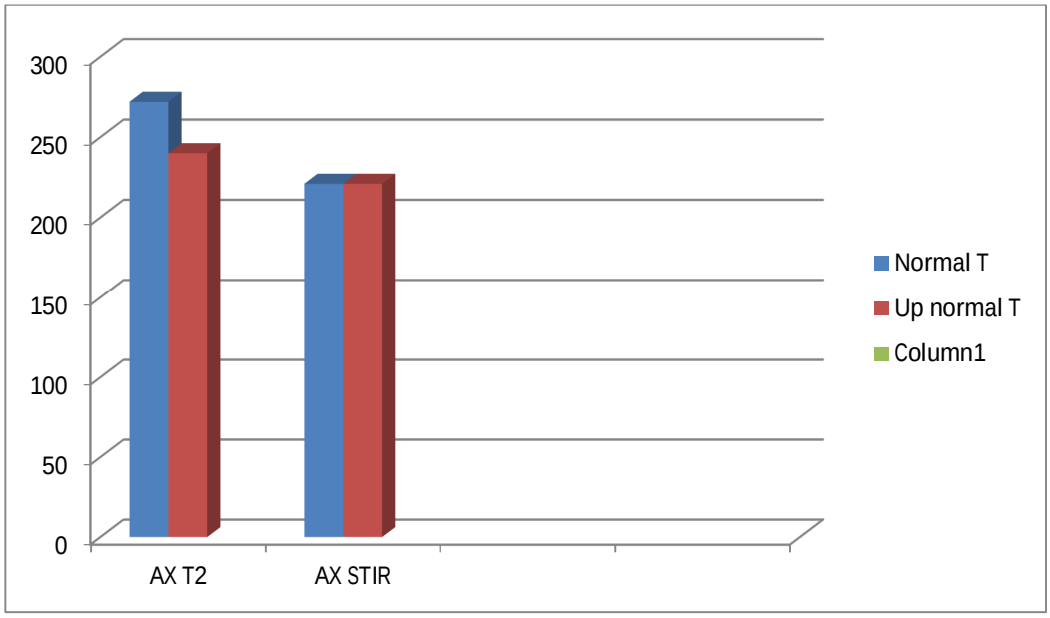

fig(6,30) Patient10 intensity chart

Normal tissues and up normal tissues were equal intensity**.** but in AXT2 technique there were different in intensities in tissues.

11. image a patient (female, aged 65) suffering of inflammation in pelvis, The patient was placed in the center of the magnet, and was inserted into.

The sequences were:

AX STIR, Ax T1, Ax T2, Coronal T2.

Diagnosis

inflammation in pelvis.

- Techniques were taken and reported in table (6,15).
- Techniques used were **AX STIR & AX T2**as shown in fig(6, 31).

Slice=10/25 area=0.5cm². PX=200

AX STIR				**AX T2**				
Up nor-tissue		Normal tissue		Up nor-tissue		Normal tissue		**Patient11**
mean	±SD	mean	±SD	mean	±SD	Mean	±SD	**parameter**
204	**12**	**70**	**12**	**648**	**18**	**626**	**8**	**Intensity**

Table(6,15)Intensities of normal & up normal tissues in AX STIR & AX T2 Techniques in patient11 image taken by GE MRI 1.5T in modern medical center

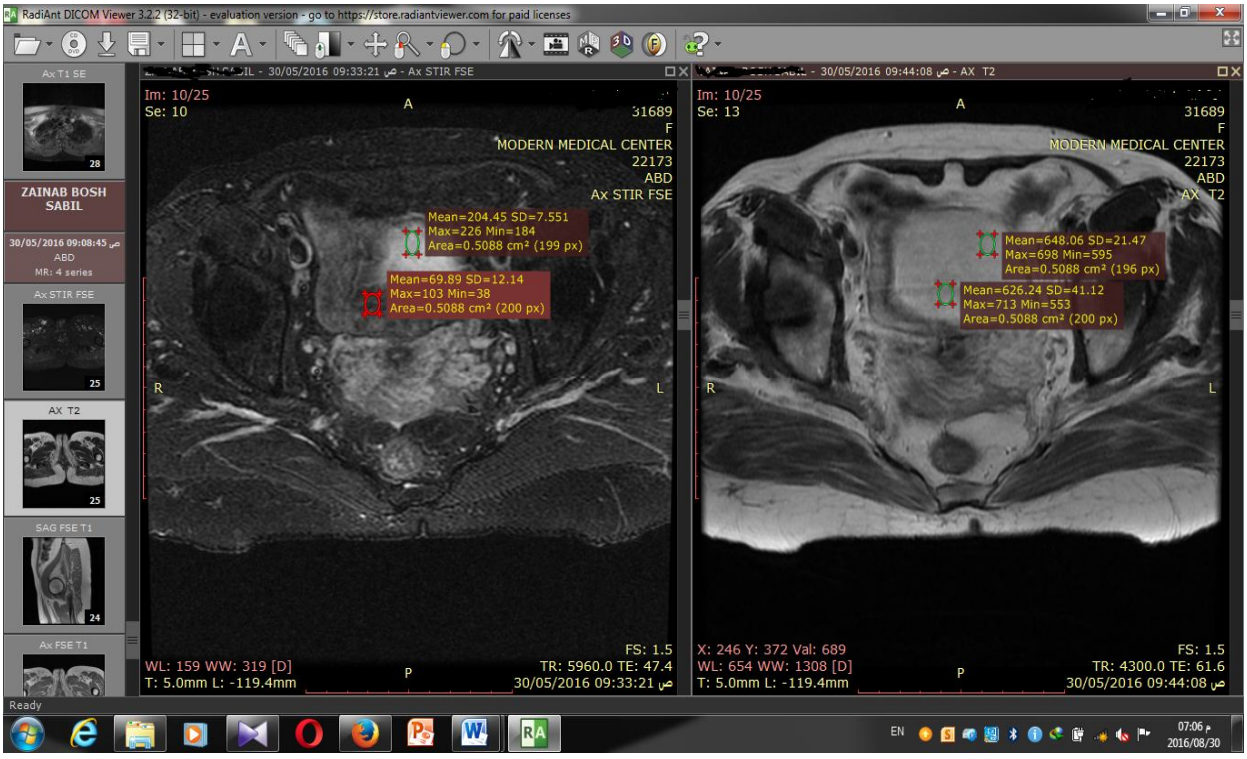

fig(6,31) comparison between AX T2 & AX STIR in patient11 image taken by GE MRI1.5T in modern medical center.

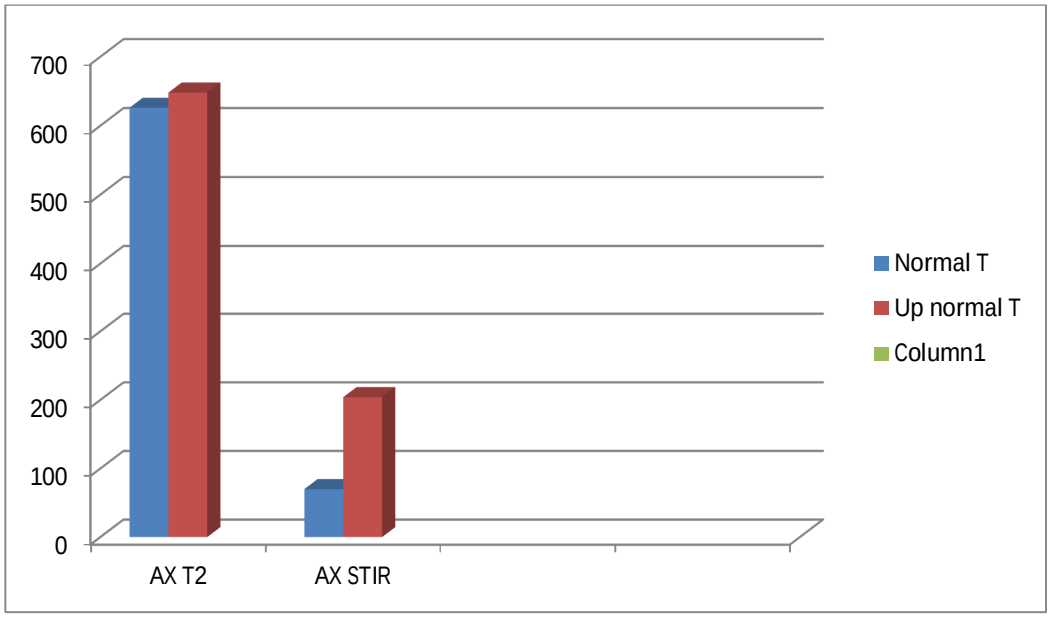

fig(6,32) Patient11 intensity chart.

As in fig (6,32) noticed that AXT2 STIR technique was more contrast & more detail than AXT2 technique.

12. image a patient (female, aged 29) suffering of inflammation in pelvis, The patient was placed in the center of the magnet, and was inserted into.

The sequences were:

AX STIR, Ax T1, Ax T2, Coronal T2.

Diagnosis

Mass tumor surrounding fluid in pelvis .

- Techniques were taken and reported in table (6,16).
- Techniques used were **AX STIR & AX T2**as shown in fig(6, 33).

Slice=1/20. area=0.5cm² PX=195

AX STIR				**AX T2**				
Up nor-tissue		Normal tissue		Up nor-tissue		Normal tissue		**Patient12**
mean	±SD	mean	±SD	mean	±SD	mean	±SD	**parameter**
370	**10**	**59**	**12**	**586**	**15**	**424**	**16**	**Intensity**

Table(6,16)Intensities of normal & up normal tissues in AX STIR & AX T2 Techniques in patient12 image taken by GE MRI 1.5T in modern medical center.

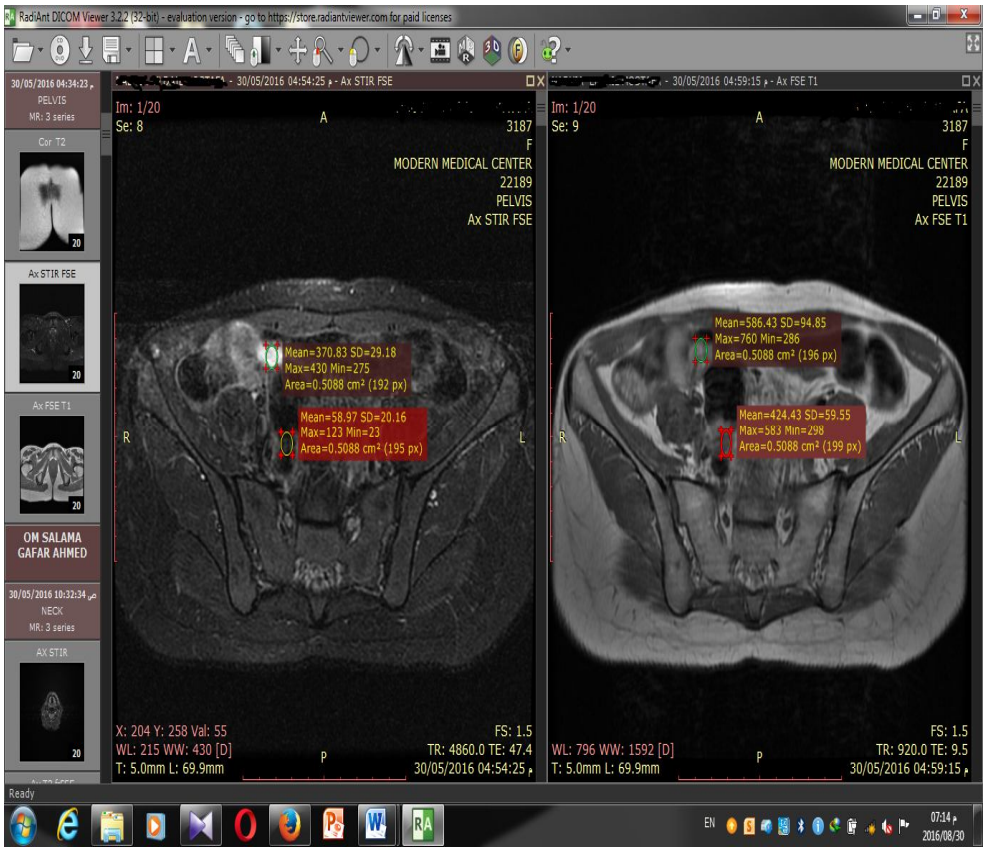

fig(6,33) comparison between AXT2 &AX STIR in patient12 image taken by GE MRI1.5T in modern medical center.

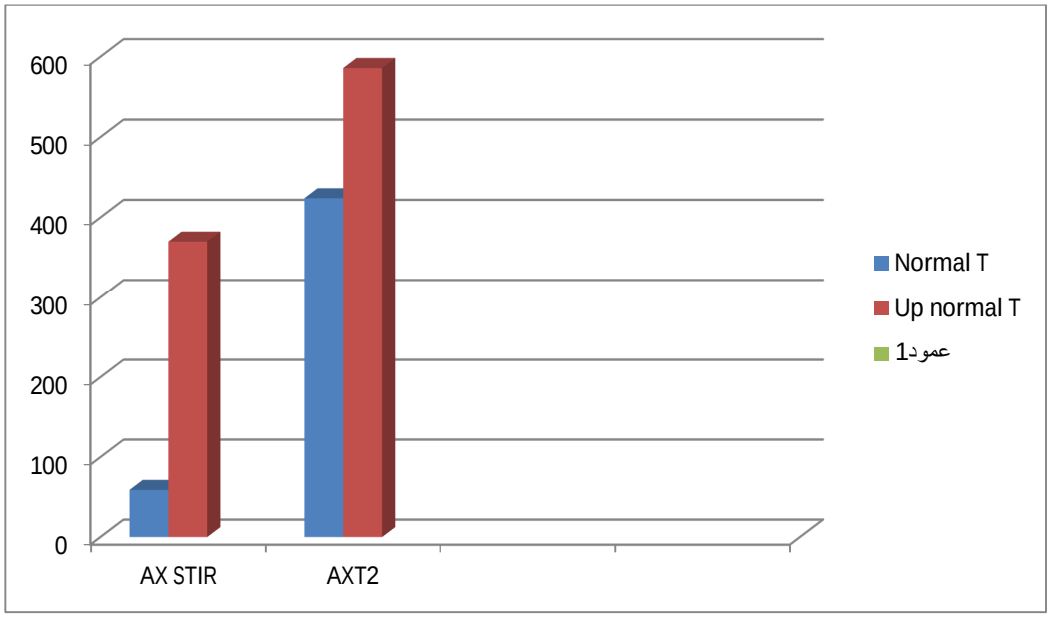

fig(6,34) Patient11 intensity chart.

As in fig (6, 34) noticed that AXSTIR technique was more contrast & more detail than AXT2 technique

Chapter Seven

7. Conclusion and recommendation

7.1 Conclusion

Wide spread clinical use of will require implementation directly on the MRI machines. This development has started recently among the major vendors.

Uses of fat suppression technique solve artifact in images that made by fat.

7.2 Recommendations

We do recommendations:

1. The modification of the exiting MRI system in Sudan by adding fat suppression technique software to be used in routine clinical applications.
2. There should be a training programs for both the doctors and staff in fat suppression technique as it highly improve the ability of MRI system as a powerful diagnostic tools.

References

1. J. Van Meter, PhD, Basic Of Magnetic Resonance Imaging, Center For Functional And Molecular Imaging, Department Of Neurology, George Town University Medical Center 2014.
2. J. Berglund, Uppsala university, "separation of water and fat, signal in magnetic resonance imaging, advanced in methods based in chemical shift" 2011.
3. A. Carrington, A.D. Mclachlan, "introduction to magnet resonance chapman and Hall, London 1967"
4. R.K. Harris, "nuclear magnetic resonance spectroscopy", Pitman, London, 1983.
5. P.C Lauterbur, "image formation by induced local interaction : example employing nuclear magnetic resonance nature 242 : 190-191 (1973).
6. S.R. Thomas, L.J. Busse, J.F. Schenck, "Gradient Coil Technology." In Magnetic Resonance Imaging,ed. by C.L. Partain, R.R. Price, J.A. Patton, M.V. Kulkarni, A.E. James Saunders, Philadelphia, 1988.
7. C.E. Hayes, W.A. Edelstein, J.F. Schenck "Radio Frequency Resonators." In Magnetic Resonance Imaging, ed. by C.L. Partain, R.R. Price, J.A. Patton, M.V. Kulkarni, A.E. James Saunders, Philadelphia, 1988
8. J.E. Roe, W.E. Prenttice, J.P. Hornak "A Multipurpose MRI Phantom Based on a Reverse Micelle Solution." Magn. Reson. Med.**35**:136-141 (1996).
9. P.S.Tofts, D. Lloyd, C.A. Clark, G.J. Barker, G.J.M. Parker, P. McConville, C. Baldock, J.M. Pope "Test Liquids for quantitative

MRI measurements of self-diffusion coefficient in vivo." Magnetic Resonance in Medicine**43**:368-374 (2000).

10. C. Poupon, B. Rieul, I. Kezel, M. Perrin, F. Poupon, J.-F. Magin "New Diffusion Phantoms Dedicated to the Study and Validation of High-Angular-Restricted Diffusion Imaging (HARDI) Models." Magnetic Resonance in Medicine**60**:1276-1283 (2008).
11. H. Kim, S.E. Taksali, S. Dufour, D. Befroy, T.R. Goodman, K.F. Petersen, G.I. Shulman, S. Caprio, R.T. Constable "Comparative MR Study of Hepatic Fat Quantification Using Single-Voxel Proton Spectroscopy, Two-Point Dixon and Three-Point IDEAL" Magnetic Resonance in Medicine**59**:521-527 (2000).
12. Metcalf, M. Auman, Ph.D., UNIV. OF CALIF., SAN FRANCISCO WITH THE UNIV. OF CALIF., BERKELEY, 2008, 135 pages; 3330865.
13. R, KOŘÍNEK, "Implementation Of Dixon Methods For Preclinical MR Imaging At High Fields" Faculty Of Electrical Engineering And Communication Department Of Theoretical And Experimental Electrical Engineering 2015.
14. L. H,Verhey.Doctorate of Philosophy Institute of Medical Science, University of Toronto MRI in the Prediction and Diagnosis of Pediatric-Onset Multiple Sclerosis: Insights from Children with Incident CNS Demyelination2012.
15. P. Peterson, "Quantification of Fat Content and Fatty Acid Composition Using Magnetic Resonance Imaging "DOCTORAL DISSERTATION, Faculty of Medicine, Lund University, Sweden, 2013.
16. P.A. Rinck, R.N. Mullre& S.B. Petersen, An Introduction To MR In Medicine, Thieme Medical Publishers, New York 1990, p, 33, 34.
17. http://mri-q.com/f-w-chemical-shift.html

18. E. M. Purcell, H. C. Torrey, and R. V. Pound. Resonance absorption by nuclear magnetic moments in a solid. Physical Review, 69(1-2):37–38, 1946.
19. P. A, Bottomley, T. H. Foster, and W. M. Leue. In vivo nuclear magnetic resonance chemical shift imaging by selective irradiation. Proceedings of the National Academy of Sciences of the United States of America, 81(21):6856–6860, 1984.
20. B. R. Rosen, V. J. Wedeen, and T. J. Brady. Selective saturation NMR imaging. Journal of Computer Assisted Tomography, 8(5):813–818, 1984.
21. A. Haase, J. Frahm, W. Hänicke, and D. Matthaei. 1H NMR chemical shift selective (CHESS) imaging. Physics in Medicine and Biology, 30(4):341–344, 1985.
22. M. S. Silver, R. I. Joseph, and D. I. Hoult. Selective spin inversion in nuclear magnetic resonance and coherent optics through an exact solution of the Bloch-Riccati equation. Physical Review A, 31(4):2753–2755, 1985.
23. F. Bloch. Nuclear induction. Physical Review, 70(7-8):460–474, 1946
24. L. G. Hanson. Is quantum mechanics necessary for understanding magnetic
resonance? Concepts in Magnetic Resonance Part A, 32A(5):329–340, 2008.
25. N. Bloembergen, E. M. Purcell, and R. V. Pound. Relaxation effects in nuclear magnetic resonance absorption. Physical Review, 73(7):679–712, 1948.
26. E. L. Hahn. Spin echoes Physical Review, 80(4):580–594, 1950.

27.H. Y. Carr and E. M. Purcell. Effects of diffusion on free precession in nuclear magnetic resonance experiments, Physical Review, 94(3):630–638, 1954.

28.J. Frahm, K. D. Merboldt, W. Hänicke, and A. Haase. Stimulated echo imaging. Journal of Magnetic Resonance (1969), 64(1):81–93, 1985.

29.E.M. Haacke, R.W. Brown, M.R. Thompson, R. Venkatesan, Magnetic Resonance Imaging : Physical

30.J. Wiley& Inc. Sons, Principles and Sequence Design, New York,. 1999. p. 422.

31. G.M. Bydder, I.R. Young, MRI: Clinical Use of the Inversion Recovery Sequence, J. Comp. Asst Tomogr. 9:659-675, 1985.

32. M.A. Bernstein, K.F. King, X.J. Zhou, Handbook of MRI Pulse Sequences, New York, Elsevier Academic Press, 2004.p. 623.

33.W.T. Dixon, Simple Proton Spectroscopic Imaging, Radiology 153: 189-194.

34.G.H. Glover, E. Schneider, Multipoint Dixon Technique for Water and Fat Proton and Susceptibility Imaging, J. Magnetic. Resonance. Imaging 1:521-530.